Physical interactions between MCM and Rad51 facilitate replication fork lesion bypass and ssDNA gap filling by non-recombinogenic functions

Cabello-Lobato, M.J.; Gonzalez-Garrido, C.; Cano-Linares, M.I.; Wong, R.P.; Yanez-Vilchez, A.; Morillo-Huesca, M.; ... ; Prado, F.

Cell Reports

Article

Physical interactions between MCM and Rad51 facilitate replication fork lesion bypass and ssDNA gap filling by non-recombinogenic functions

Graphical abstract

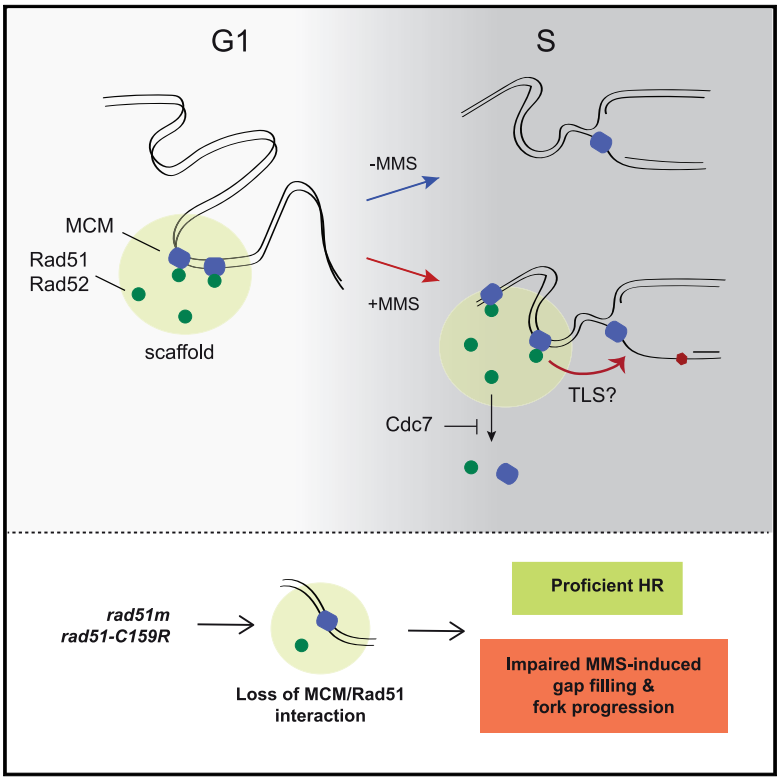

Highlights

- Rad51 and Rad52 interact with MCM in a nuclease-insoluble nucleoprotein scaffold
- MCM/Rad51/Rad52 accumulation is regulated by cell cycle and replicative DNA damage
- Cdc7 prevents Rad51/Rad52 release from the scaffold under replicative DNA damage
- MCM/Rad51 promotes MMS-induced gap filling and fork progression by non-HR processes

Authors

María J. Cabello-Lobato, Cristina González-Garrido, María I. Cano-Linares, ..., Román González-Prieto, Helle D. Ulrich, Félix Prado

Correspondence

felix.prado@cabimer.es

In brief

Cabello-Lobato et al. find that MCM interacts dynamically with Rad51 and Rad52 within a nuclease-insoluble nucleoprotein scaffold. These interactions are established in G1 and maintained in the S phase by Cdc7 in the presence of replication-blocking lesions to assist stressed forks through non-recombinogenic functions.

Cabello-Lobato et al., 2021, Cell Reports *36*, 109440
July 27, 2021
https://doi.org/10.1016/j.celrep.2021.109440

CellPress

Cell Reports

CellPress
OPEN ACCESS

Article

Physical interactions between MCM and Rad51 facilitate replication fork lesion bypass and ssDNA gap filling by non-recombinogenic functions

María J. Cabello-Lobato,[1,3,4] Cristina González-Garrido,[1,3] María I. Cano-Linares,[1] Ronald P. Wong,[2] Aurora Yáñez-Vílchez,[1] Macarena Morillo-Huesca,[1] Juan M. Roldán-Romero,[1] Marta Vicioso,[1] Román González-Prieto,[1,5] Helle D. Ulrich,[2] and Félix Prado[1,6,*]

[1]Centro Andaluz de Biología Molecular y Medicina Regenerativa–CABIMER, Consejo Superior de Investigaciones Científicas; Universidad de Sevilla; Universidad Pablo de Olavide; Seville, Spain
[2]Institute of Molecular Biology (IMB), Mainz, Germany
[3]These authors contributed equally
[4]Present address: Manchester Cancer Research Centre, Division of Cancer Sciences, University of Manchester, Manchester M20 4GJ, UK
[5]Present address: Department of Cell and Chemical Biology, Leiden University Medical Center, Leiden, the Netherlands
[6]Lead contact
*Correspondence: felix.prado@cabimer.es
https://doi.org/10.1016/j.celrep.2021.109440

SUMMARY

The minichromosome maintenance (MCM) helicase physically interacts with the recombination proteins Rad51 and Rad52 from yeast to human cells. We show, in *Saccharomyces cerevisiae*, that these interactions occur within a nuclease-insoluble scaffold enriched in replication/repair factors. Rad51 accumulates in a MCM- and DNA-binding-independent manner and interacts with MCM helicases located outside of the replication origins and forks. MCM, Rad51, and Rad52 accumulate in this scaffold in G1 and are released during the S phase. In the presence of replication-blocking lesions, Cdc7 prevents their release from the scaffold, thus maintaining the interactions. We identify a *rad51* mutant that is impaired in its ability to bind to MCM but not to the scaffold. This mutant is proficient in recombination but partially defective in single-stranded DNA (ssDNA) gap filling and replication fork progression through damaged DNA. Therefore, cells accumulate MCM/Rad51/Rad52 complexes at specific nuclear scaffolds in G1 to assist stressed forks through non-recombinogenic functions.

INTRODUCTION

Replicative stress is a major source of genomic instability, which is associated with cancer and genetic diseases (Hills and Diffley, 2014). Cells are endowed with different mechanisms to deal with DNA lesions that hinder the advance of replication forks. The DNA damage tolerance (DDT) response facilitates replication fork progression through damaged DNA, postponing the repair of blocking lesions for later stages to timely complete genome duplication. The homologous recombination (HR) machinery has multiple and critical roles in this process through mechanisms that are mostly error free, in contrast to translesion synthesis (TLS) mechanisms, which can be mutagenic (Branzei and Psakhye, 2016; Prado, 2014, 2018). HR proteins escort the fork under unperturbed conditions (Alabert et al., 2014; González-Prieto et al., 2013; Hashimoto et al., 2010; López-Contreras et al., 2013) and assist replication forks in response to replicative stress. In mammalian cells, the recombinase RAD51 is required for the formation and protection of reversed forks as intermediates to promote replication fork bypass of blocking lesions (Bhat and Cortez, 2018; Zellweger et al., 2015). Reversed forks are rarely detected in yeast cells treated with the alkylating agent methyl methanesulfonate (MMS) or UV light, which cause DNA blocking lesions (Giannattasio et al., 2014; Lopes et al., 2006). However, yeast Rad51 also prevents the accumulation of single-stranded DNA (ssDNA) fragments at the forks (Hashimoto et al., 2010; Lopes et al., 2006), and together with its mediator Rad52 are required for fork progression in the presence of alkylated bases (Alabert et al., 2009; González-Prieto et al., 2013; Vázquez et al., 2008).

It has long been established in the yeast *Saccharomyces cerevisiae* that HR proteins are required to fill in the stretches of ssDNA generated during DNA replication in the presence of DNA adducts (Gangavarapu et al., 2007; Jachymczyk et al., 1977; Prakash, 1981; Resnick et al., 1981). This process requires multiple recombination factors, including Rad51 and Rad52, and relies on the transient formation of sister chromatid junctions (SCJs) through strand-exchange reactions (Branzei et al., 2008; Liberi et al., 2005; Mankouri et al., 2007; Vanoli et al., 2010). In addition, we have recently shown that Rad51 and Rad52 facilitate TLS through non-recombinogenic functions (Cano-Linares et al., 2021). In *S. cerevisiae*, the repair of these ssDNA gaps occurs post-replicatively at DNA regions that are

spatially separated from replication forks (González-Prieto et al., 2013; Wong et al., 2020).

Previous studies in *Schizosaccharomyces pombe* and human cells showed that Rad51 and Rad52 physically interact with the minichromosome maintenance (MCM) helicase complex in the absence and presence of drugs that impair DNA replication (Bailis et al., 2008; Shukla et al., 2005). The MCM helicase is a conserved ring-shaped complex formed by six related subunits (Mcm2 to Mcm7 in *S. cerevisiae*) with essential roles in DNA replication. The loading of MCM at chromatin occurs during late mitosis and G1 and requires the initial binding of the origin recognition complex (ORC) to a replication origin, followed by the recruitment of Cdc6 and the final entry of an MCM/Cdt1 heptamer. In this pre-replicative complex (pre-RC), the MCM helicase is loaded as an inactive head-to-head dimer that encircles dsDNA. This complex is activated during S phase through a process that requires the activities of the cyclin- and Dbf4-dependent kinases (Cdc28 and Cdc7 in *S. cerevisiae*, respectively) and the binding of the replication factors Cdc45 and GINS (forming the CMG complex). During these steps, the double hexamer is split, and each active ring is opened and re-closed around the leading ssDNA template to promote DNA unwinding as the CMG complex translocates during replication elongation (Deegan and Diffley, 2016; Labib, 2010; Li and O'Donnell, 2018). Remarkably, the number of MCM complexes loaded at chromatin exceeds the number of replication origins and ORCs by a factor of 10 to 50. These excess MCM complexes spread over the surrounding chromatin where they have different roles in response to replication stress (Das and Rhind, 2016; Hyrien, 2016).

We show in the yeast *S. cerevisiae* that Rad51 and Rad52 display dynamic interactions with MCM in a nuclease-insoluble scaffold in which MCM, but not Rad51, seems to be directly bound to DNA. Binding to this scaffold is regulated through the cell cycle in a DNA-damage-dependent manner. In unperturbed cells, they accumulate in G1 and are released during S phase; however, in the presence of replication stress, Cdc7 prevents the release of Rad51 and Rad52 from the scaffold, thus, maintaining their association with MCM. Functionally, the interaction between MCM and Rad51 promotes replication fork advance and ssDNA gap repair through non-recombinogenic mechanisms.

RESULTS

MCM interaction with Rad51 and Rad52 is regulated by the cell cycle, DNA damage, and Cdc7

To determine whether the interactions of MCM with Rad51 and Rad52 are conserved in *S. cerevisiae*, we performed coimmunoprecipitation (CoIP) experiments using a GFP-tagged allele of Mcm4, which did not affect cell growth. Rad51 coimmunoprecipitated with Mcm4, regardless of whether the lysates were pretreated with the nucleases MNase I (Figure 1A) or benzonase (Figure 1B), indicating that the interaction was not mediated by DNA. This CoIP also showed an association of Mcm4 with Rad52 (Figure 1B). However, the absence of Rad52 did not prevent the formation of the MCM/Rad51 complex, despite Rad52 being required for Rad51 binding to replication forks and ssDNA lesions (González-Prieto et al., 2013). In fact, the amount of precipitated Rad51 increased in *rad52Δ* cell extracts (Figure 1A, right panel), suggesting dynamic interactions between Rad51, Rad52, and MCM. Next, we performed the CoIP analysis in asynchronous cultures treated or not for 2 h with either MMS or hydroxyurea (HU), which causes deoxyribonucleotide triphosphate (dNTP) depletion. The MCM/Rad51 interaction was observed in the absence and presence of either DNA-damaging agent, although it was stronger in response to MMS (Figures 1C and 1D).

Cdc7 is a major regulator of MCM activity (Labib, 2010). To determine whether the interaction between Rad51 and Mcm4 requires the kinase activity of Cdc7, we used an allele of *CDC7* (*cdc7-as3*) that is sensitive to the ATP analog inhibitor 1NMPP1 (Wan et al., 2006). Because Cdc7 is essential for replication initiation, the inhibitor was added 30 min after G1 release, and the interaction was tested 60 min later. The experiment was performed in the presence of MMS to maintain cells with comparable cell-cycle profiles. The addition of 1NMPP1 prevented Rad51 from coimmunoprecipitating with Mcm4, indicating that the MCM/Rad51 association requires the continuous kinase activity of Cdc7 (Figure 1E). The requirement of Cdc7 for replication initiation can be bypassed by a mutation in Mcm5 (*mcm5-bob1*) (Hardy et al., 1997). Likewise, Cdc7 activity was not required to maintain the MCM/Rad51 interaction both in *cdc7-as3 mcm5-bob1* treated with an inhibitor and in *cdc7Δ mcm5-bob1* cells in the presence of MMS or HU (Figures 1D, 1E, and S1A), suggesting that Cdc7 maintains the MCM/Rad51 interaction in response to DNA damage by acting upon the MCM complex. When these experiments were repeated in cells released in the absence of DNA damage, the MCM/Rad51 interaction was detected in unperturbed S/G2 cells only after over-exposure of the western blot (Figure 1F, lanes 2 and 3). Furthermore, the *mcm5-bob1* mutation was not sufficient to maintain the MCM/Rad51 interaction in the absence of DNA damage (Figure S1B). Rad51 also coimmunoprecipitated with Mcm4 in G1-arrested cells (Figure 1G), even though there is no Cdc7 activity in that phase (Weinreich and Stillman, 1999). Interestingly, Mcm4 is modified under conditions that promote its interaction with Rad51 (Figures 1F, 1G, and S1C), in part because of phosphorylation, as determined by phosphatase λ treatment (Figure S1D). Altogether, our CoIP analyses show an interaction between MCM and Rad51 in G1 that is lost during unperturbed S/G2; however, in the presence of replicative DNA damage, the kinase activity of Cdc7 maintains the interaction.

The MCM/Rad51 complex localizes to a nuclease-insoluble nuclear scaffold

To determine the location of the MCM/Rad51 interaction, we first separated, by cell lysis and centrifugation, the soluble (supernatant) and insoluble (pellet containing the chromatin) fractions from cells growing asynchronously under unperturbed conditions; proper fraction was confirmed by western blots against histone H4 (insoluble fraction) and Pgk1 (soluble fraction) (Figure 2A, left panel). The amount of Rad51 interacting with Mcm4 was much greater in the insoluble, than in the soluble, fraction, even though both factors were more abundant in the soluble fraction (Figure 2A, right panel).

Nuclease digestion of the pellet solubilizes most of the chromatin; however, there is a residual nuclease-insoluble chromatin

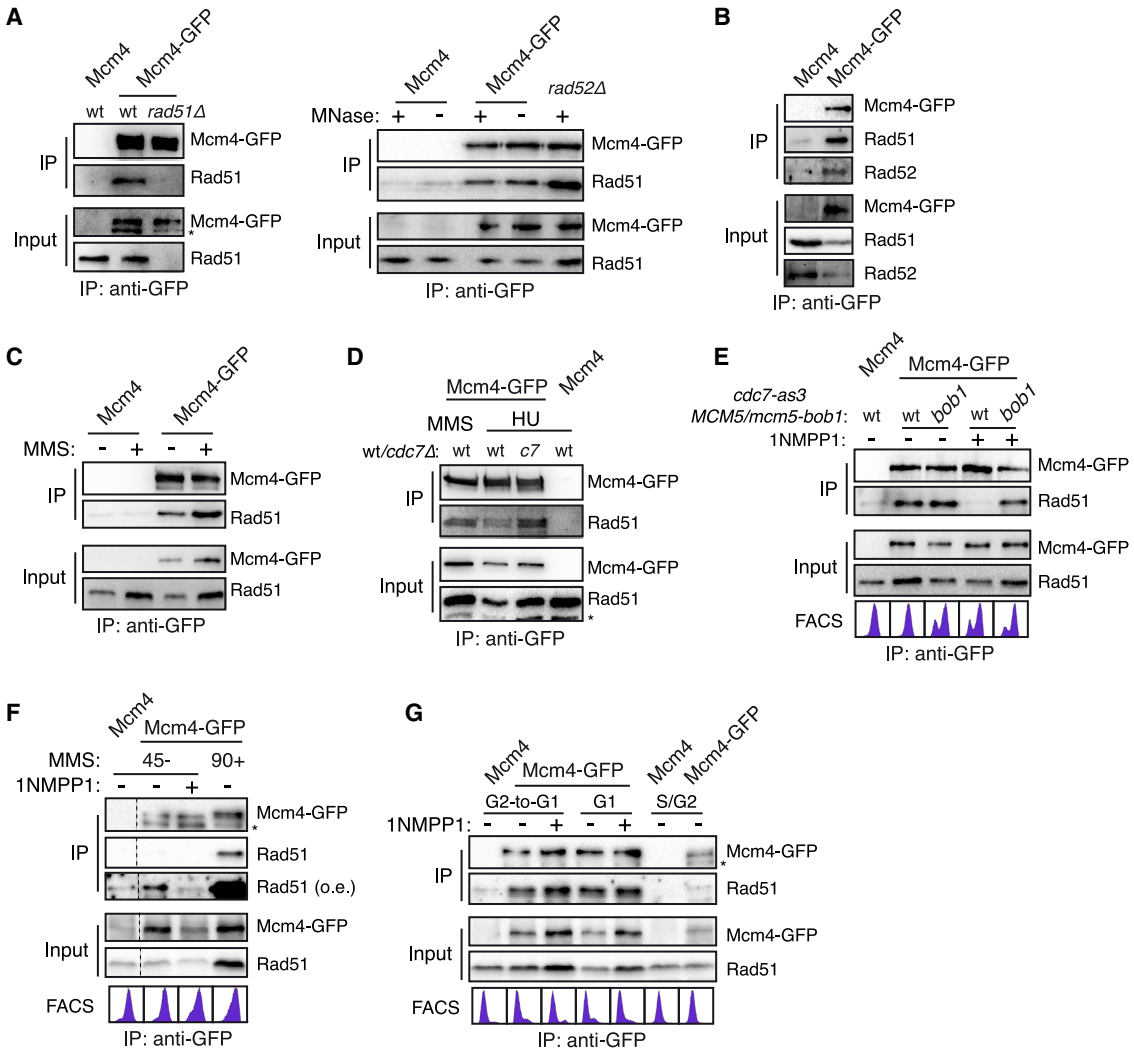

Figure 1. MCM interacts with Rad51 and Rad52 through mechanisms regulated by cell cycle, DNA damage, and Cdc7

(A) Rad51 interacts with Mcm4, independent of Rad52. CoIP was performed in asynchronous cultures.

(B) Mcm4 interacts with Rad52. Interactions were detected regardless of whether extracts had been treated or not with MNase I (A) or benzonase (B). CoIP was performed in asynchronous cultures.

(C) Mcm4 interacts with Rad51, both with and without 0.015% MMS for 2 h. CoIP was performed in asynchronous cultures.

(D) Mcm4 interacts with Rad51 in *cdc7Δ mcm5-bob1* and wild-type cells treated with 0.2 M HU for 2 h. Wild-type cells treated with 0.025% MMS for 2 h were included as controls. CoIP was performed in asynchronous cultures.

(E) The Mcm4/Rad51 interaction in cells released into MMS during the S phase depends on Cdc7 kinase activity, and *mcm5-bob1* bypasses that requirement. *cdc7-as3* cells were synchronized in the G1, released into the S phase in the presence of 0.015% MMS for 90 min, and treated with 15 μM 1NMPP1 30 min after G1 release.

(F) Mcm4/Rad51 interaction is eliminated during an unperturbed S phase. G1-synchronized cells were released in the absence or presence of 0.015% MMS for 45 and 90 min, respectively, and were treated or not with 15 μM 1NMPP1 30 min after G1 release (−MMS). An over-exposure (o.e.) of the Rad51 gel is shown.

(G) The Mcm4/Rad51 interaction occurs in G1, independent of Cdc7 activity. The analysis was performed in G1-arrested cells, either coming from G1 and released into fresh medium with α-factor and 15 μM 1NMPP1 60 min later (G2-to-G1) or maintained in G1 for 30 min with and without an inhibitor (G1). Cells synchronized in G1 and released into fresh medium for 60 min were included as controls (S/G2).

Physical interactions of MCM with Rad51 and Rad52 were determined by immunoprecipitation of Mcm4-GFP and western blot analyses. All experiments were repeated at least twice with similar results. The asterisks indicate a degradation product. Dashed lines indicate spliced images.

fraction that precipitates with the scaffold protein Top2, the checkpoint protein Rad53, and the replication factors ORC, Dbf4, and Sgs1 (Frei and Gasser, 2000; Pasero et al., 1999). To determine in what fraction Rad51 and MCM were present under the conditions in which they interact, the pellets obtained after fractionation of G1-arrested and MMS-released cells were digested with benzonase, and nuclease-soluble and insoluble fractions were analyzed by centrifugation, followed by western blot. A control with undamaged cells from an asynchronous culture was included for comparison. As expected, nuclease

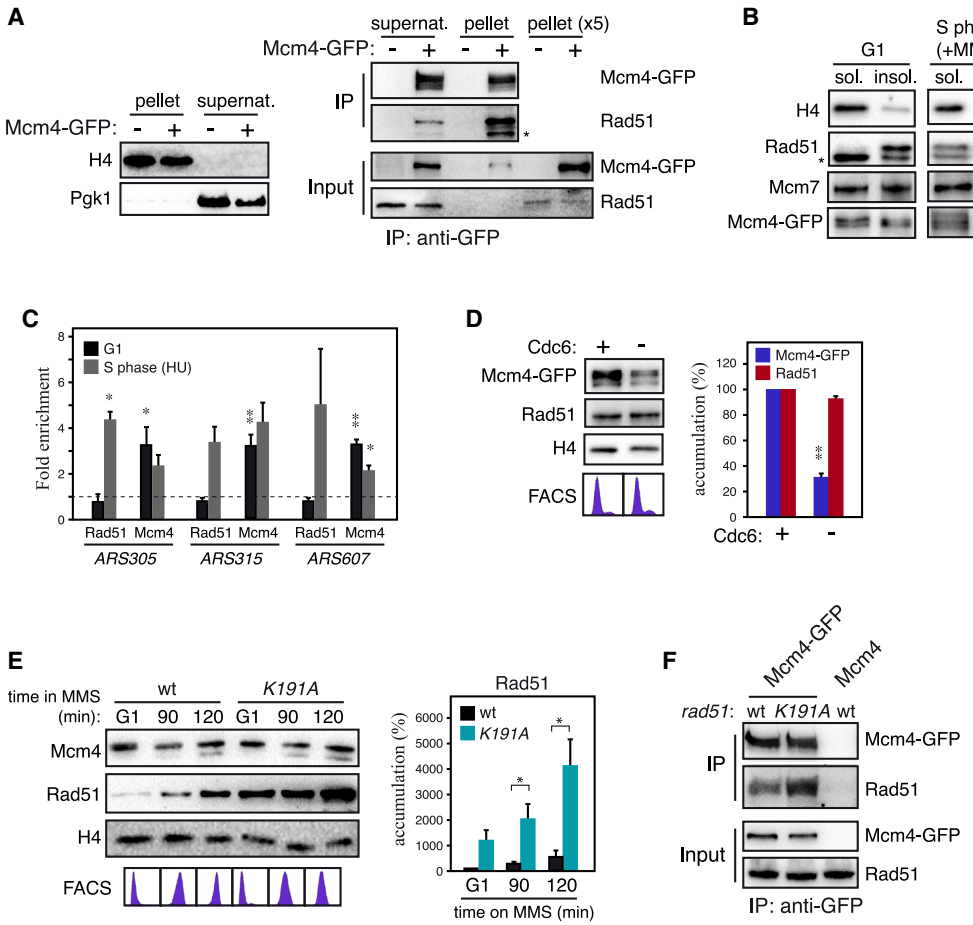

Figure 2. The MCM/Rad51 complex localizes to a nuclease-insoluble nuclear scaffold

(A) Immunoprecipitation of Rad51 with Mcm4-GFP using MNase-I-treated lysates from insoluble (pellet) and soluble (supernatant) fractions from asynchronously growing cells (right panels). Similar cell equivalents of the insoluble and soluble fractions were loaded for the fractionation controls (left panels) and CoIP samples (right panels). For the input of the CoIP samples, one and five equivalents of the soluble fraction were loaded for the insoluble fraction. The asterisk indicates an unspecific band as determined in a *rad51Δ* strain (data not shown). The experiments were repeated twice with similar results.

(B) Rad51 and MCM accumulate in a nuclease-insoluble fraction both in cells arrested in G1 and in cells released in the presence of 0.025% MMS for 120 min. An unperturbed asynchronous culture was included as a control. The pellet obtained after cell fractionation was further fractionated into nuclease-soluble and -insoluble fractions by treatment with benzonase and centrifugation, and the amount of histone H4, Rad51, Mcm7, and Mcm4-GFP was determined by western blot. The asterisk indicates an unspecific band as determined in a *rad51Δ* strain (data not shown). The experiments were repeated twice with similar results.

(C) MCM/Rad51 interaction is prevented at the pre-RC. Rad51 and Mcm4-GFP accumulation at replication origins in cells synchronized in G1 and released into the S phase for 1 h in the presence of 0.2 M HU. The means ± SEM of three independent ChIP experiments are shown. One and two asterisks represent significant differences with the untagged strain; *$p < 0.05$ and **$p < 0.01$; two-tailed Student's t test.

(D) *CDC6* expression is required for MCM, but not for Rad51, accumulation in the insoluble fraction in G1, as determined in *GAL::CDC6* cells synchronized in G1 under conditions of Cdc6 repression. The amount of Mcm4 and Rad51 (normalized to H4) left in the insoluble fraction in Cdc6-depleted cells relative to Cdc6-expressing cells is shown. The means ± SEM from three independent experiments are shown. Two asterisks represent a significant difference with the Cdc6-expressing strain; **$p < 0.01$; one-sample t test.

(E) The DNA-binding domain of Rad51 is dispensable for its accumulation in the insoluble fraction. G1-synchronized *rad51-K191A* and wild-type cells were released into the S phase in the presence of 0.025% MMS. The binding of MCM and Rad51 to the insoluble fraction was determined by cell fractionation and western blot analyses (see Figure S1I for fractionation controls). Histone H4 was used to normalize the amount of each protein. The mean ± SEM from five independent experiments are shown. One asterisk represents a significant difference; *$p < 0.05$; two-tailed Student's t test.

(F) MCM/Rad51 interaction augments in a *rad51-K191A* mutant. CoIP was performed in asynchronous cultures treated with 0.025% MMS for 2 h. Similar results were obtained in three independent experiments.

treatment released most of the chromatin, as determined by the enrichment of histone H4 in the soluble fraction (Figure 2B). Rad51 remained in the nuclease-insoluble pellet. Indeed, the helicase MCM, which is released to the solubilized fraction in unperturbed asynchronous cultures (Figure 2B) (Liang and Stillman, 1997; Pasero et al., 1999), was also partially retained in the nuclease-insoluble pellet in G1- and MMS-treated S-phase cells (Figure 2B).

These results suggest that MCM and Rad51 accumulate in a nuclease-insoluble fraction under conditions that promote their interaction. To determine whether MCM and Rad51 bind to DNA in this fraction, we first used chromatin immunoprecipitation (ChIP) to probe their accumulation at three different replication origins in G1-arrested cells. As a positive control, their presence was also monitored at forks arrested in the early S phase by means of an HU treatment. Whereas both Mcm4 and Rad51 accumulated at stalled forks in the S phase, only Mcm4 was detected at the origins in G1 (Figure 2C). Neither Mcm4 nor Rad51 significantly accumulated at three different positions close to *ARS305* in G1 (Figure S1E). These results indicate that the MCM/Rad51 interaction does not occur at the pre-RC in G1.

To determine whether MCM was bound to DNA in the insoluble fraction, we analyzed its accumulation in the absence of Cdc6, essential for MCM loading onto DNA (Cocker et al., 1996). For that, *GAL1::CDC6* cells were synchronized in G1 in the presence of glucose to repress the expression of Cdc6. Under these conditions, cells were unable to exit G1. This approach reduced the amount of Mcm4 in the insoluble fraction to ~30% (Figures 2D and S1F), suggesting that most MCM in this fraction is bound to DNA. Notably, the accumulation of Rad51 was unaffected under these conditions (Figure 2D). Indeed, neither Rad51 nor Rad52 was required for Mcm4 accumulation in this fraction in G1 (Figures S1G and S1H).

To test whether Rad51 was bound to DNA in the insoluble fraction, we employed a mutant (*rad51-K191A*) defective in DNA binding (Fung et al., 2006; Van Komen et al., 2000; Li et al., 2007; Morgan et al., 2002; Sung and Stratton, 1996) and followed its accumulation both in G1 and during S phase in the presence of MMS. The amount of Rad51-K191A in the insoluble fraction was strongly increased as compared with the wild-type protein (Figures 2E and S1I), suggesting that Rad51 is preferentially bound to a nuclear scaffold in a DNA-independent manner and that Rad51 is dynamically exchanged between that scaffold and DNA. Finally, we observed that the increase of Rad51 at that nuclear scaffold in the *rad51-K191A* mutant augmented its interaction with MCM (Figure 2F), further supporting the dynamism of these interactions. Altogether, these results suggest that MCM and Rad51 are independently recruited and interact dynamically in a nuclease-insoluble nucleoprotein scaffold. Although Rad51 associates to that compartment in a DNA- and MCM-independent manner, MCM seems to be bound to DNA.

Cell cycle, DNA damage, and Cdc7 regulate the accumulation of MCM, Rad51, and Rad52 in the nuclear scaffold

To better understand the regulation of the MCM/Rad51/Rad52 interactions, we followed their binding to the insoluble fraction under various conditions (Figure 3; see Figure S2 for fractionation controls). We first analyzed their binding during the cell cycle under unperturbed conditions. As previously reported, Mcm4 accumulated in the insoluble fraction in G1 and was transiently lost during the S phase (Figure 3A) (Aparicio et al., 1997; Liang and Stillman, 1997; Tanaka et al., 1997). Rad51 and Rad52 displayed a similar pattern of binding during the cell cycle (Figures 3A and S3A). That reduction in binding to the insoluble fraction during replication was not due to lower levels of total protein (Figure S3B).

As we anticipated in Figure 2E, MCM, Rad51, and Rad52 were not released from the insoluble fraction during S/G2 in the presence of MMS; indeed, the amount of Rad51 and Rad52 increased with time (Figures 3B and S3A). It is worth noting that Mcm4 remained bound, even at very late times in MMS, during which bulk DNA was largely replicated (Figure 3B, FACS profiles), indicating that its maintenance was not due to replication inhibition.

These results suggest a functional connection between the physical interactions of MCM with Rad51 and Rad52 and their binding to the insoluble fraction. To further explore that possibility, we studied the genetic requirements of that binding. Fractionation analyses showed that Rad52 is not required for Rad51 binding to the insoluble fraction; indeed, the amount of Rad51 at that fraction increased in *rad52Δ* (Figure 3C). Next, we studied the role of Cdc7 in cells released into the S phase in the presence of MMS. Rad51 and Rad52 were lost from the insoluble fraction in the absence of Cdc7 kinase activity (Figures 3D and S3C), and that phenotype was suppressed by the *mcm5-bob1* mutation (Figure 3E). In the case of MCM, the results were not conclusive. MCM was maintained in the insoluble fraction after Cdc7 inhibition in most kinetics (Figure 3D); however, it was released to the same extent as Rad51 in some cases (5 of 16; see Figure S3D), suggesting a partial requirement of Cdc7 for a stable binding of MCM to the insoluble fraction. Overall, our results suggest that the formation of an MCM/Rad51/Rad52 complex is mechanistically linked to the binding of their components to a nuclear scaffold.

Cdc7 is required to maintain Rad51 in the insoluble fraction, independent of the MCM/Rad51 interaction

Restricting Rad52 expression to G2/M prevents Rad51 from binding to MMS-induced ssDNA gaps and interferes with its repair (González-Prieto et al., 2013), suggesting that the recruitment of the recombination proteins to ssDNA gaps during DDT must occur during the S phase. This is a substantial mechanistic distinction from double-strand break (DSB)-induced HR; in which, Rad51 and Rad52 are recruited to ssDNA independent of DNA replication (Alabert et al., 2009; Barlow and Rothstein, 2009). To better understand this process, we performed a search for *rad51* mutants sensitive to MMS and resistant to ionizing radiation (IR). We obtained five *rad51* alleles in centromeric plasmids that were tested for their ability to interact with MCM as a putative mechanism to explain the coupling between replication and Rad51 binding to ssDNA gaps during DDT. One of them (*rad51m*) was defective in its interaction with MCM (Figure S4A). To rule out the possibility that these phenotypes were due to its plasmid location, we reproduced them in a strain in which chromosomal *RAD51* was replaced with the *rad51m* allele (Figures 4A and 4B).

The kinetics of MCM and Rad51 binding to the insoluble fraction, both in the absence and presence of MMS, were similar in *rad51m* and wild-type cells (Figures 4C, 4D, S4B, and S4C). These results confirm that the MCM/Rad51 interaction is not required for its recruitment to the insoluble fraction (Figure 2D) and suggest that Cdc7 maintains the MCM/Rad51 interaction

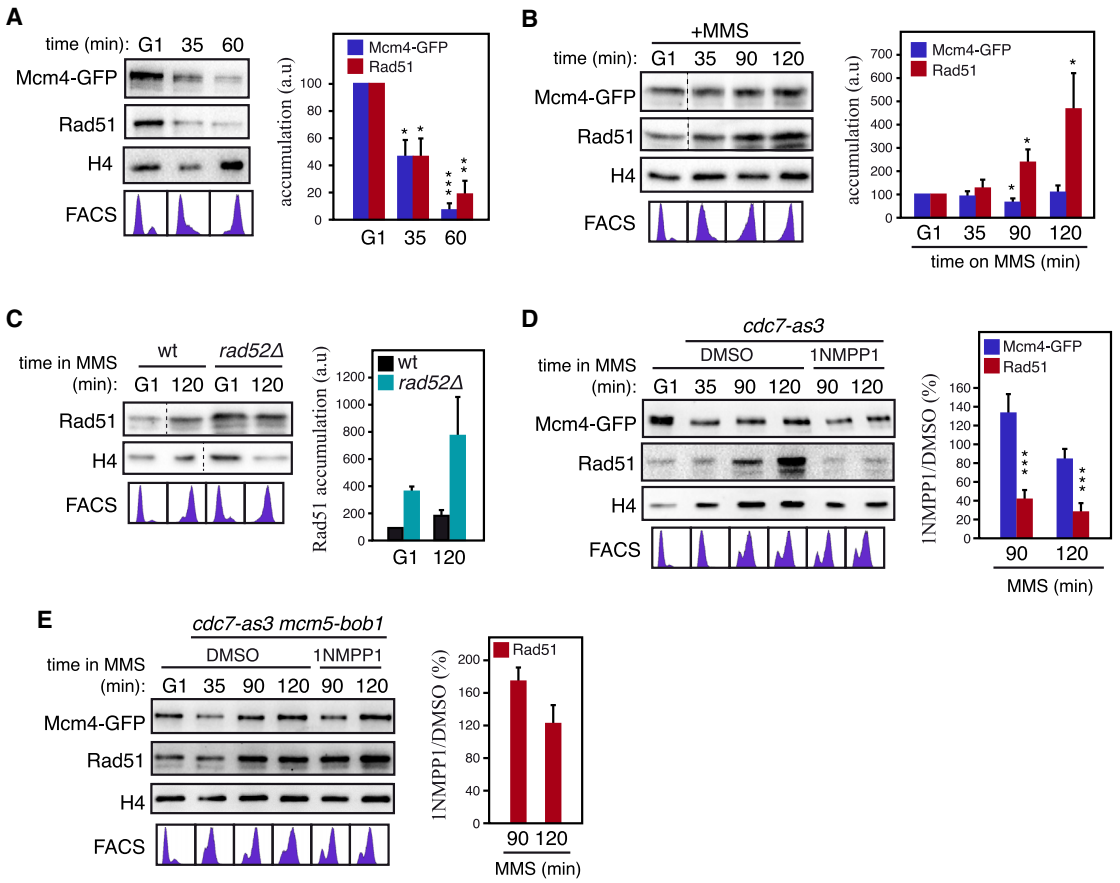

Figure 3. Cell cycle, DNA damage, and Cdc7 regulate the accumulation of MCM, Rad51, and Rad52 in the insoluble fraction

(A) Mcm4 and Rad51 accumulate in the insoluble fraction in G1 and are released during the S phase.

(B) Mcm4 and Rad51 are maintained in the insoluble fraction during the S phase in the presence of 0.025% MMS.

(C) Rad52 is not required for Rad51 binding to the insoluble fraction in G1 and MMS-released cells.

(D) Inhibition of Cdc7 kinase activity prevents the maintenance of Rad51 in the insoluble fraction in response to DNA damage. G1-synchronized cells were released into the S phase in the presence of 0.025% MMS; they were treated with 15 μM 1NMPP1 35 min after G1 release.

(E) The *mcm5-bob1* mutation bypasses the requirement of Cdc7 for Rad51 maintenance in the insoluble fraction under replicative stress. G1-synchronized cells were released into the S phase in the presence of 0.025% MMS; they were treated with 15 μM 1NMPP1 35 min after G1 release.

MCM and Rad51 binding to the insoluble fraction was determined by cell fractionation and western blot. See Figure S2 for fractionation controls (A–E). Dashed lines indicate spliced images. Histone H4 was used to normalize the amount of each protein. The mean of 4 (A), 11 for Mcm4-GFP and 14 for Rad51 (B), 2 (C and E) and 11 for 90-min, and 6 for 120-min (D) independent experiments are plotted. Either the SEM (A, B, and D) or range (C and E) are shown. Values are normalized to G1 (A–C) or to the absence of the inhibitor (D and E), taking as 100. Statistically significant differences relative to G1 (A and B) or to the absence of the inhibitor (D) are shown; *p < 0.05, **p < 0.01, ***p < 0.001; one-sample t test.

by preventing Rad51 from dissociating from the nuclear scaffold. In agreement with that, the binding of Rad51 to the insoluble fraction was reduced to a similar extent in *rad51m* and wild-type cells upon Cdc7 inhibition (Figures 4E and S4D). Therefore, Cdc7 is required to maintain Rad51 in the nuclear scaffold in the presence of replicative DNA damage but is, independent of the MCM/Rad51 interaction.

The interaction between MCM and Rad51 facilitates the replication of damaged DNA

DNA content analyses revealed defects in replication fork progression in the presence of MMS in the *rad51m* mutant (Figure 4D, FACS profiles). To better characterize that phenotype, we followed DNA replication at shorter time intervals. The *rad51m* mutant did not display replication defects under unperturbed conditions (Figures S5A and S5B); however, it displayed a gradual delay in the replication of MMS-damaged DNA, which became evident at late times after G1 release (Figure 5A). The absence of Cdc7 activity also affected replication fork progression, which was severely aggravated in *rad51m cdc7-as3* cells (Figure 4E, FACS profiles). Likewise, *rad51m* and *cdc7-as3* single mutants exhibited a delay in completing DNA replication and entering into the following cell cycle after MMS treatment, whereas the *rad51m cdc7-as3* double mutant was unable to complete replication (Figure 5B). These replicative defects were confirmed by pulse field gel electrophoresis (PFGE), in which only completely replicated chromosomes can enter into the gel (Figures 5C and S5C).

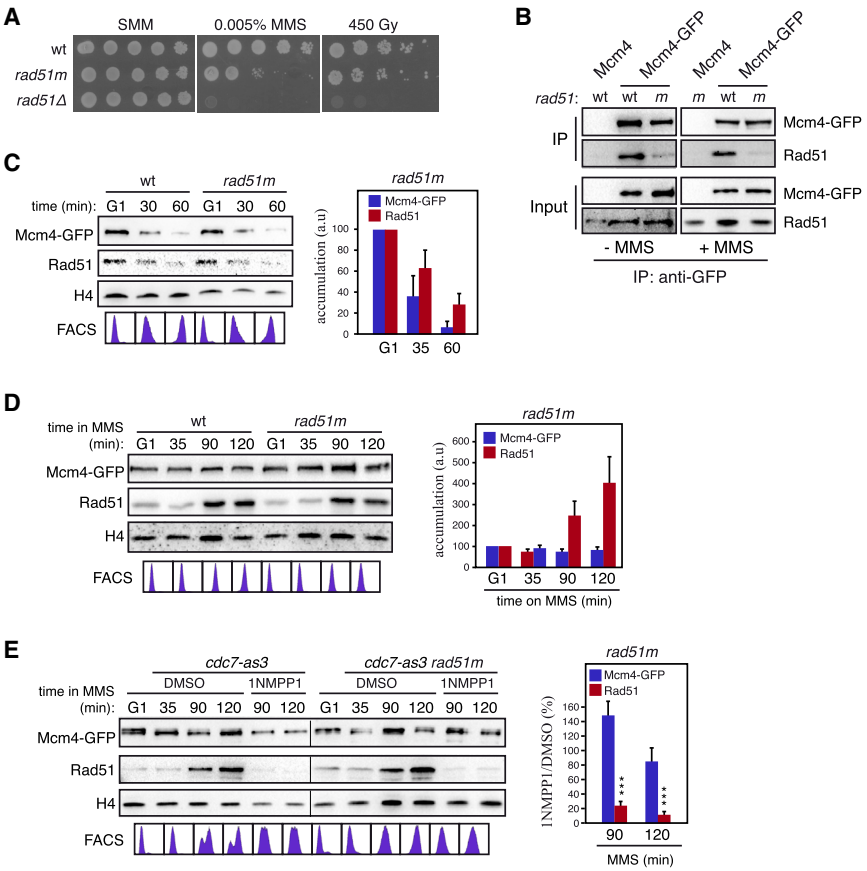

Figure 4. Cdc7 is required to maintain Rad51 in the insoluble fraction, independent of the MCM/Rad51 interaction

(A) MMS and IR sensitivity of *rad51m*, *rad51Δ*, and wild-type cells.

(B) The Rad51m mutant protein is defective in its interaction with MCM, as determined by CoIP from asynchronous cultures treated or not with 0.025% MMS for 2 h. The experiment was repeated twice with similar results.

(C–E) Mcm4 and Rad51 accumulate in the insoluble fraction in G1 and are released during the S phase in *rad51m* cells (C), unless they are released in the presence of 0.025% MMS (D). (E) Inhibition of Cdc7 kinase activity prevents the maintenance of Rad51 in the insoluble fraction in *rad51m* cells released into 0.025% MMS and treated with 15 μM 1NMPP1 35 min after G1 release. MCM and Rad51 binding to the insoluble fraction was determined by cell fractionation and western blot. See Figure S4B–S4D for fractionation controls. Histone H4 was used to normalize the amount of each protein. The mean of 2 (C), 6 (D), and 7 (E) independent experiments are plotted. Either the range (C) or SEM (D are E) are shown. Values are normalized to G1 (C and D) or the absence of inhibitor (E), taking as 100. Three asterisks represent a significant difference relative to the absence of inhibitor; ***$p < 0.001$; one-sample t test.

Next, we used DNA fiber assays to analyze the replication fork speed (Figure 5D). We observed no significant difference in replication tract lengths between wild-type and *rad51m* cells 30 min after G1 release under unperturbed condition. Replication tract lengths in both strains decreased to a similar extent 30 min after release into MMS compared with the unperturbed conditions. However, although wild-type cells significantly increased replication tract lengths 60 min after G1 release into MMS, *rad51m* mutant cells were unable to accelerate DNA synthesis at the same time point (Figure 5D, left graph). Interestingly, we observed clusters of smaller replication tracts after 30 min in MMS, leading to a decrease in inter-origin distances (Figure 5D, right graph). This is probably due to firing of dormant origins upon replication stress, which has been described in mammalian cells (Ge et al., 2007). Although inter-origin distances remained unchanged in wild-type cells from 30 to 60 min after release into MMS, this parameter was further significantly reduced in the *rad51m* mutant (Figure 5D, right graph). These data suggest that the *rad51m* mutant is partially defective in supporting replication fork progression through MMS-damaged template but compensates for that defect by firing an increasing number of dormant origins. This might explain why the replication defect of *rad51m* is aggravated in the absence of Cdc7 activity (Figure 5B).

To demonstrate that the replication defects of the *rad51m* mutant were associated with its inability to interact with MCM, we forced the MCM/Rad51 interaction in the *rad51m* mutant by co-expressing Mcm4 and Rad51m tagged with GFP and GBP (GFP-binding protein), respectively. Tagging Rad51 with GBP caused strong MMS sensitivity (Figure 5E), suggesting a loss of functionality in recombinational repair, as previously reported for Rad51-GFP (Waterman et al., 2019). Rad51m-GBP cells progressed more slowly than did Mcm4-GFP and wild-type cells in the presence of MMS (Figure 5F). Importantly, co-expression of Rad51m-GBP and Mcm4-GFP partially restored the speed of DNA replication (Figure 5F, left). Likewise, cells co-expressing Rad51m-GBP and Mcm4-GFP reached G2/M earlier than cells expressing only Rad51m-GBP did after resuming replication after MMS treatment (Figure 5F, right), suggesting that the interaction between MCM and Rad51 facilitates DNA replication in the presence of blocking DNA lesions.

DNA fiber analyses showed that the Mcm4-GFP chimera partially restores the Rad51m-GBP defect in replication through damaged DNA by accelerating the elongation rate as inferred from the increase in the replication tract length from 30 to 60 min (Figure 5G, left graph). This increase in fork progression was concomitant with a suppression in the firing of additional replication origins (Figure 5G, right graph). Of note, the Mcm4-GFP chimera partially restored the replication defects of the *rad51m-GBP* mutant but suppressed neither the MMS sensitivity nor the HR defect (Figures 5E and S5D), suggesting that the MCM/Rad51 complex does not require the recombinational function of Rad51 to promote replication fork progression.

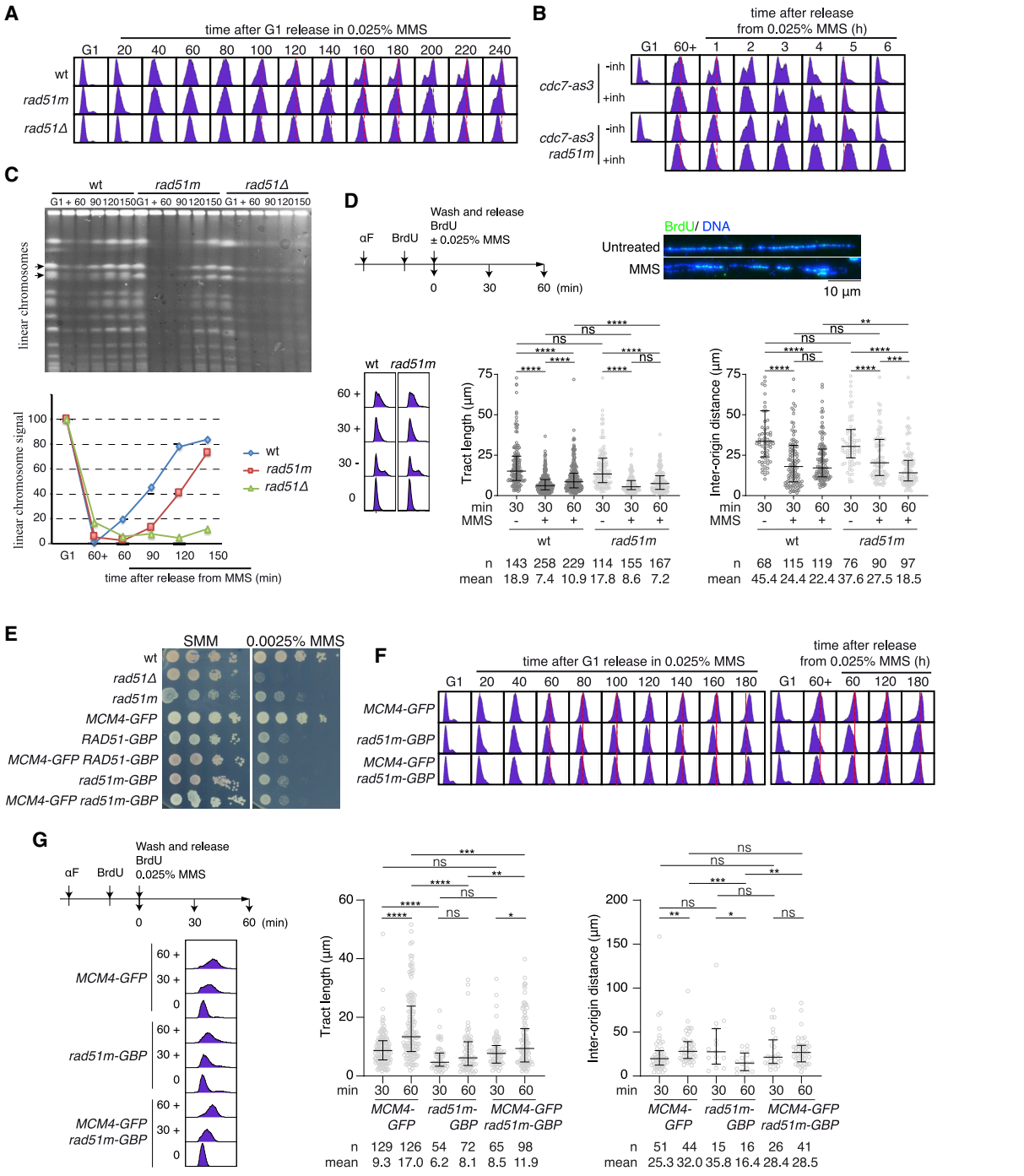

Figure 5. The interaction between MCM and Rad51 facilitates for DNA replication in the presence of MMS

(A and B) Cell-cycle progression of the indicated strains synchronized in G1 and released in the presence of 0.025% MMS for different times (A) or released into 0.025% MMS for 1 h and then into fresh medium after MMS inactivation (B). In (B), cells were treated with 15 μM 1NMPP1 for 30 min after G1 release and every 2 h to keep Cdc7 inactive. α-Factor was also added every 2 h to prevent cells from entering a new cycle.

(C) Cell-cycle progression determined by PFGE analysis of the indicated strains synchronized in G1, released into 0.025% MMS for 1 h, and then, into fresh medium after MMS inactivation. Quantified chromosomes are shown with arrows. The plot shows the mean signal relative to G1, taken as 100.

(D) Replication tract length (left) and inter-origin distance (right) in *rad51m* and wild-type cells growing under unperturbed and MMS conditions, as determined by DNA fiber analysis. G1-synchronized cells were incubated with BrdU for 15 min, washed twice, and released into the S phase in the presence of BrdU with or without 0.025% MMS. Bars represent the median and the 25th and 75th percentiles. Statistically significant differences according to Mann-Whitney tests are

(legend continued on next page)

The *rad51m* mutant is proficient in HR but partially defective in the repair of MMS-induced ssDNA gaps at Rad52-associated DNA repair centers

To determine whether the MCM/Rad51 interaction was relevant for MMS-induced DNA damage repair, we followed the resolution of MMS-induced Rad52 foci, which can be detected at the end of the S and G2 phases (González-Prieto et al., 2013). For that, G1-synchronized cells were released into the S phase in the presence of 0.033% MMS for 1 h and, then, into fresh medium after MMS inactivation to allow for DNA damage repair. About 50% of the *rad51m* and wild-type cells accumulated Rad52 foci 1–2 h after MMS inactivation (Figure S6A). Importantly, although the percentage of wild-type cells with Rad52 foci dropped to ~5% 4–5 h later (85% resolution), it only dropped to 25% in *rad51m* cells (45% resolution) (Figures 6A, left panel, and S6A). A similar defect was observed when we calculated the fluorescence signal at foci per cell, which integrates the percentage of cells that retain foci as well as the number and intensity of the foci (Figures 6A, right panel, and S6B). This result suggests that ssDNA lesions are not efficiently repaired in the *rad51m* mutant. To further confirm that, we followed the kinetics of replication protein A (RPA) foci formation and resolution. The RPA complex (formed by the Rfa1–3 subunits) covers ssDNA lesions, regardless of the mechanism of repair. The efficiency of ssDNA gap filling, inferred from both the percentage of cells with foci and the RPA signal per cell at the end of the time course relative to the peak during the time course, was severely compromised in the *rad51m* mutant (Figures 6B, S6C, and S6D); indeed, RPA foci resolution was affected even at a dose of 0.01% MMS (Figure S6E), which had no effect on *rad51m* viability (Figure S6F). The defect in RPA foci resolution was greater than the one observed with Rad52 foci, likely because of detection levels, as suggested by the fact that the peak of cells with RPA foci was approximately twice that of the peak of Rad52 foci (compare Figures 6A and 6C, left panels).

To determine whether the defect in DNA repair of the *rad51m* mutant was specific for MMS, we followed the formation and resolution of RPA foci in cells irradiated in G1 with 35 Gy and released into the S phase for different times (Figures 6C, S6G, and S6H). Although the repair was slower in the *rad51m* mutant than it was in the wild-type cells at the beginning of the kinetics (Figures 6C and S6H, right panels; compare the RPA signal at 2 h), the efficiency of gap repair was similar in both strains, as determined by the percentage of cells with foci and the signal intensity at the end of the kinetics (Figure 6C, left and right panels, respectively). Therefore, the *rad51m* mutant was defective in the repair of MMS-induced ssDNA gaps but not of IR-induced DSBs, even though the lethality induced with 35 Gy was greater than that induced with 0.033% MMS (Figure 6D). Notably, this defect in ssDNA gap filling was not associated with a significant loss of viability (Figure S6F).

To determine what molecular step was compromised in the *rad51m* mutant, we first tested the interaction of Rad51 with Rad52. The amount of Rad52 bound to Rad51 was strongly increased in the mutant as compared with that of the wild-type cells (Figure 6E), further supporting the dynamism of the MCM/Rad51/Rad52 interactions. Next, we analyzed Rad51 binding to MMS-damaged DNA by chromatin-endogenous cleavage (ChEC). In this approach, cells expressing a chimera of Rad51 fused to MNase I (Rad51-MN) are permeabilized with digitonin and treated with Ca^{2+} ions for different time points to activate the nuclease; then, total DNA is analyzed by agarose gel electrophoresis. The rationale behind this approach is that the chimera will generate a detectable cut only if it is targeted to an uncut DNA fragment (González-Prieto et al., 2013, 2021). Although the binding of Rad51 to the insoluble fraction is independent of Rad52 (Figure 3C), Rad52 is essential for MMS-induced DNA cleavage by Rad51-MN (González-Prieto et al., 2013). Rad51m-MN and Rad51-MN displayed similar DNA digestion profiles (Figure 6F), suggesting that the interaction with MCM is not required for Rad51 binding to ssDNA lesions. Similar conclusions were obtained by analyzing Rad51 binding to HU-stalled replication forks in *rad51m* and wild-type cells by ChIP (Figure S6I).

The repair of MMS-induced DNA lesions by HR is associated with the formation of SCJs, which can be detected as X-shaped structures by two-dimensional (2D) electrophoresis in *sgs1Δ* cells that are defective in their dissolution (Liberi et al., 2005). The *sgs1Δ* and *sgs1Δ rad51m* cells displayed similar kinetics of X-shaped molecule accumulation (Figure 6G), indicating that the interaction with MCM is not required for the DNA strand-exchange activity of Rad51.

Finally, we measured HR using an unequal sister chromatid exchange (uSCE) system (Fasullo and Davis, 1987). For that, exponentially growing cells were treated either with MMS for 4 h or with IR, and the frequency of recombinants was determined before and after DNA damage. The *rad51m* mutant was not significantly affected in HR in response to MMS or IR (Figure 6H). Therefore, the interaction of Rad51 with MCM is not required for the recombinational repair of ssDNA lesions and DSBs. Altogether, these results indicate that the *rad51m* mutant is impaired in a non-recombinogenic mechanism of ssDNA gap filling.

We could not use the Mcm4-GFP/Rad51m-GBP system to demonstrate that the *rad51m* defect in DNA repair is associated with the disruption of the MCM/Rad51 interaction because the Rad51m-GBP chimera is defective in HR. Because the *rad51m* allele contains five amino acid substitutions (Figure S7A), we decided to determine which one is responsible for disrupting the MCM/Rad51 interaction. The *rad51-C159R* mutant displayed a similar defect in MCM binding as the *rad51m* mutant had (Figure S7B). In comparison with *rad51m*,

shown; $^{**}p < 0.01$, $^{***}p < 0.001$, $^{****}p < 0.0001$. Cell cycle profiles and representative images of DNA fibers stained with antibodies against BrdU (green) and single-stranded DNA (blue) from wild-type cells 30 min after G1 release are shown.

(E) MMS sensitivity of the indicated strains.

(F) Cell-cycle progression in the presence (left) and after treatment for 1 h with 0.025% MMS (right) of cells expressing Mcm4-GFP, Rad51m-GBP, or both.

(G) Replication tract length (left) and inter-origin distance (right) in *MCM4-GFP*, *rad51m-GBP*, and *MCM4-GFP rad51m-GBP* cells growing in the presence of 0.025% MMS as indicated in (D). The experiments were repeated twice with similar results.

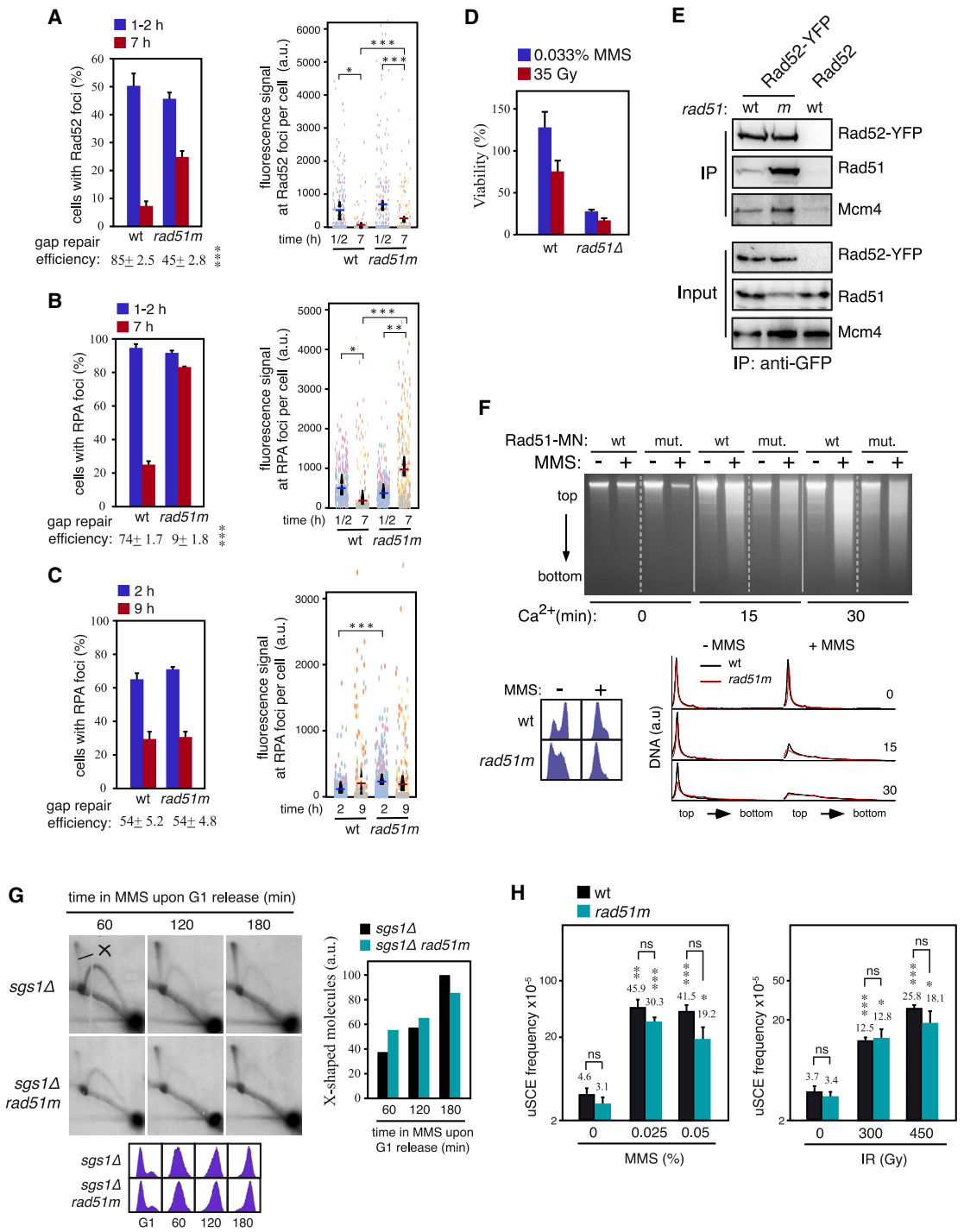

Figure 6. The *rad51m* mutant is proficient in HR but partially defective in the repair of MMS-induced ssDNA gaps at Rad52-associated DNA repair centers

(A–C) DNA repair efficiency of *rad51m* and wild-type cells, as determined by analyzing the formation and resolution of MMS-induced Rad52-YFP (A), MMS-induced Rfa1-YFP (B), and IR-induced Rfa1-YFP (C) foci. In (A) and (B), G1-synchronized cells were released into the S phase in the presence of 0.033% MMS for 1 h and then into fresh medium after MMS inactivation. In (C), cells were synchronized in G1, irradiated with 35 Gy, and released into the S phase. Complete kinetics are shown in Figures S6A, S6C, and S6G. The percentage of cells with foci (left panels) and the fluorescent signal at foci per cell (right panels) at 1/2 (peak) and 7/9 hours from the time course was determined with MetaMorph software. The efficiency of ssDNA gap repair was calculated as (100 − percentage of cells with foci at the end of the time course × 100)/maximal percentage of cells with foci during the time course. Color dots represent independent experiments.

(D) Cell viability of strains treated with either 0.033% MMS for 1 h or 35 Gy as determined by the number of colony-forming cells before and after DNA damage.

(legend continued on next page)

the *rad51-C159R* mutant was less sensitive to MMS (Figure S7C), which might explain the mild sensitivity of the *rad51m* mutant to acute doses of both MMS and IR (Figure S6F). However, and importantly, both mutants displayed similar defects in the repair of MMS-induced Rad52 foci (Figures S7D). Therefore, the disruption of the MCM/Rad51 interaction is genetically linked to a point mutation that causes a non-recombinogenic defect in MMS-induced DNA damage repair.

DISCUSSION

Here, we have studied the regulation and biological meaning of the physical interactions between the helicase MCM and the recombination factors Rad51 and Rad52 in *S. cerevisiae.* We observed that Rad51 and Rad52 display dynamic interactions with MCM complexes located outside of the replication origins and forks in a nuclease-insoluble scaffold in which Rad51 accumulates in a MCM- and DNA-binding-independent manner. These interactions are detected in G1 and are lost in S/G2, unless DNA replication occurs in the presence of replicative DNA lesions; in this case, Cdc7 maintains the integrity of the MCM/Rad51/Rad52 complex by preventing the release of Rad51/Rad52 from the scaffold. Functionally, the MCM/Rad51 interaction facilitates the fork advance and ssDNA repair through non-recombinogenic activities.

Cell cycle, DNA damage, and Cdc7 regulate the physical interactions between Rad51/Rad52 and MCM in a nuclease-insoluble scaffold

MCM, but not Rad51, was detected at replication origins in G1, whereas both factors accumulated at the forks (Figure 2C). This indicates that the MCM/Rad51 association is prevented at the pre-RC and that Rad51 binds to the fork once replication is initiated. The interaction of MCM with Rad51 and Rad52 was rarely detected in an unperturbed S phase (Figure 1F), suggesting that it is also prevented at the replication forks. Indeed, Rad51 requires Rad52 to bind to the fork (González-Prieto et al., 2013) but not to MCM (Figures 1A). This raises a question about the location and molecular nature of these interactions. Our fractionation analysis showed that Rad51 and MCM accumulate and interact with each other in a nuclease-insoluble fraction (Figures 2A and 2B). In principle, this fraction might be nuclease-insoluble chromatin. However, Rad51 requires neither its DNA binding activity nor MCM to accumulate in that fraction or to interact with MCM (Figures 2D, 2F, 4C, and 4D), indicating that Rad51 does not associate directly with DNA. In contrast to Rad51, the amount of MCM is strongly reduced in the insoluble fraction if its loading onto DNA is impaired by repressing Cdc6 expression (Figure 2D). This suggests that MCM binds to nuclease-insoluble chromatin, where it interacts with Rad51. These data point to a model in which Rad51 and Rad52 interact with DNA-bound MCM in a nucleoprotein scaffold (Figure 7). These interactions would be highly dynamic considering their enrichment in the absence of some of the interacting partners: Rad51 with both MCM and the scaffold in *rad52Δ* (Figures 1A and 3C) and *rad51-K191R* mutants (Figures 2E and 2F), and Rad51 with Rad52 in the *rad51m* mutant (Figure 6E).

MCM helicases are assembled at every cell cycle during mitosis using newly synthesized subunits (Braun and Breeden, 2007), loaded onto replication origins at the end of mitosis and G1 (Aparicio et al., 1997; Donovan et al., 1997; Liang and Stillman, 1997; Tanaka et al., 1997), and prevented from binding to chromatin during the rest of the cell cycle (Nguyen et al., 2001). Because we did not detect Rad51 at the replication origins, the association between Rad51 and MCM may involve an excess of helicases that are loaded in G1 at replication origins and spread to the surrounding chromatin. However, genome-wide analyses have shown that MCM is concentrated at replication origins (Das et al., 2015; Wyrick et al., 2001), suggesting that this MCM/Rad51/nucleoprotein scaffold may not be associated with specific DNA positions and/or is not detected by those genomic approaches as a consequence of their insolubility. Alternatively, MCM might accumulate and interact with Rad51 and Rad52 outside of the chromatin fiber, considering that ~30% of Mcm4 remains in the insoluble fraction after repressing Cdc6. Future biochemical and genomic analyses will be required to address this point.

Remarkably, this nuclease-insoluble fraction is characterized by the presence of Top2, Rad53, Sgs1, the ORC, and the Cdc7-regulator Dbf4 (Frei and Gasser, 2000; Pasero et al., 1999), which are involved in replication fork stability under replication stress (Branzei and Foiani, 2010). In mammalian cells, replication origins and components of the pre-RC, including MCM, are associated during G1 and early S phases with the nuclear scaffold, defined as a salt-resistant or nuclease-insoluble nuclear fraction (Hesketh et al., 2015; Wilson and Coverley, 2013). According to those data, the DNA would be spooled through static replication machinery, and the newly synthesized DNA would be extruded as two loops (Wilson and Coverley, 2013). In a hypothetical similar frame, the yeast MCM/Rad51/Rad52 complexes would remain located near the forks during replication for assistance under conditions of replicative stress (Figure 7).

(E) The amount of Rad51 that interacts with Rad52 augments in the *rad51m* mutant. CoIP was performed in asynchronous cultures treated with 0.025% MMS for 2 h. The experiments were repeated twice with similar results.
(F) The Rad51m mutant protein is proficient in binding to replicative ssDNA lesions, as determined by ChEC analysis of exponentially growing cells incubated with 0.05% MMS for 2 h. Total DNA from cells permeabilized and treated with Ca^{2+} for different times is shown, as well as the DNA content and DNA digestion profiles. The experiments were repeated twice with similar results.
(G) The Rad51m mutant protein is proficient in the SCJ formation, as determined by 2D gel analysis of X-shaped molecules in cells synchronized in G1 and released in the presence of 0.033% MMS. The amount of X-shaped molecules (spike), relative to the total amount of molecules, with the highest value set at 100, is shown. The experiments were repeated twice with similar results.
(H) uSCE frequency in *rad51m* and wild-type cells upon exposure to increasing doses of MMS for 4 h (left) and IR (right).
The means ± SEM of three independent experiments are shown. *p < 0.05, **p < 0.01, ***p < 0.001; unpaired two-tailed Student's t test (A–D and H).

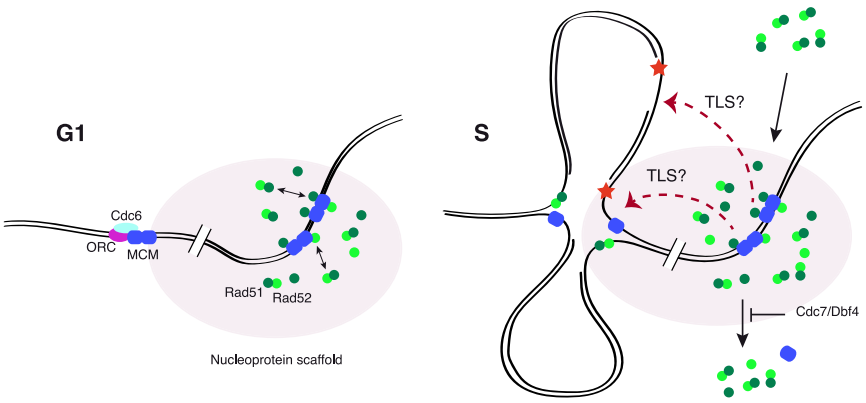

Figure 7. The interaction of MCM with Rad51 facilitates replication fork advance and ssDNA gap repair in the presence of MMS

Rad51 and Rad52 interact physically and dynamically with MCM in a nuclease-insoluble scaffold where Rad51 accumulates in a MCM- and DNA-binding-independent manner. Rad51/Rad52-interacting MCM helicases are loaded onto DNA in G1 and spread out of replication origins, although we cannot formally rule out that the interactions involve MCM molecules located outside of the DNA. MCM, Rad51, and Rad52 accumulate in G1 and are released during unperturbed replication. In the presence of replication-blocking lesions, MCM remains and Rad51/Rad52 augments through the recruitment of additional molecules and the kinase activity of Cdc7, which prevents Rad51/Rad52 (and partially, MCM) from releasing the scaffold. These physical interactions help stressed replication forks by facilitating their advance and the filling of ssDNA gaps by non-HR mechanisms, which might include TLS (dashed arrows).

The interactions of Rad51 with both MCM and the nuclease-insoluble fraction during replicative DNA damage require Cdc7 activity (Figures 1E and 3D), suggesting that they are mechanistically linked. In this regard, the fact that the Rad51m mutant binds to the insoluble fraction (Figures 4C and 4D) demonstrates that the integrity of the MCM/Rad51 complex is not required for the binding of Rad51 to that scaffold. Rather, it suggests that the binding of Rad51 to that scaffold is a pre-requisite for its interaction with MCM and that the Cdc7 activity helps to maintain Rad51 and Rad52 in that scaffold under replicative stress. How Cdc7 performs that task is currently unknown, but the fact that Rad51 and Rad52 fall off the insoluble fraction after inactivating Cdc7 in cells that have already triggered early origins and progressed through the S phase (Figures 3D and S3C) suggests that it is not associated with its replication-initiation function. The Cdc7 requirement to maintain Rad51 in the insoluble fraction was observed even in the *rad51m* mutant (Figure 4E), indicating that the mechanism by which Cdc7 facilitates Rad51 binding to this nuclear fraction is independent of the MCM/Rad51 interaction. However, the requirement of Cdc7 activity for Rad51 binding to the insoluble fraction was bypassed by a mutation in a MCM complex subunit (*mcm5-bob1*) (Figure 3E). This suggests that Cdc7 performs this task by acting upon MCM, likely by generating a structural context that facilitates Rad51 binding; actually, this function might not be specific for Rad51 and Rad52, as suggested by the requirement of Cdc7 to maintain the replisome-associated factor Tof1 in the insoluble fraction and the bypass of this requirement by the *mcm5-bob1* mutation (Bastia et al., 2016). The *mcm5-bob1* mutation causes a conformational change in the MCM helicase, which rescues the lethality associated with the lack of Cdc7 (Hoang et al., 2007). Mcm2 phosphorylation by Cdc7 weakens its interaction with Mcm5, suggesting a potential mechanism for helicase opening and ssDNA extrusion during replication initiation that would be mimicked by the Mcm5-bob1 protein (Bruck and Kaplan, 2015). However, it is unlikely that Cdc7 facilitates Rad51 binding to the insoluble fraction by generating a local accumulation of ssDNA because the DNA binding activity of Rad51 is dispensable for its binding to this fraction. Alternatively, MCM phosphorylation might facilitate the formation of a nucleoprotein scaffold or phase-separated liquid compartment as those reported recently at DSB repair centers (Kilic et al., 2019; Miné-Hattab et al., 2021)

Functional role of the MCM/Rad51 interaction in replication fork advance and ssDNA repair

A remarkable finding of this work is the cell-cycle kinetics of Rad51 and Rad52 binding to the nuclear scaffold: they accumulate in G1 and are released during the S phase, even though HR is inactive in G1 and active in the S phase (Heyer et al., 2010). This kinetics parallels that of the helicase MCM (Aparicio et al., 1997; Liang and Stillman, 1997; Tanaka et al., 1997); indeed, MCM, Rad51, and Rad52 also display similar patterns of binding to this scaffold in the presence of MMS, remaining bound to damaged DNA (Figures 3A, 3B, and S3A). As previously discussed, this kinetics of binding might facilitate physical interactions between Rad51 and Rad52 with MCM helicases located outside of pre-RCs and forks. This population of helicases vastly outnumbers the number of replication origins (Donovan et al., 1997), raising a question about their functionality that has been partially resolved by their role in activating dormant origins under replicative stress (Ge et al., 2007; Ibarra et al., 2008; Maki et al., 2011). We have ruled out a role for the MCM/Rad51 interaction in the activation of dormant origins, which actually are triggered in the *rad51m* mutant. We propose that Rad51 and Rad52 aggregate, together with excess MCM helicases (and likely additional factors), at specific nucleoprotein scaffolds in G1 for replication assistance. These aggregates would be removed during the S phase under unperturbed conditions, likely to avoid the toxicity of Rad52/Rad51/MCM-DNA interactions (Shah et al., 2010). In response to replicative DNA damage, Cdc7 would maintain those physical interactions to assist stressed replication forks by facilitating their advance and the repair of the stretches of ssDNA generated during lesion bypass (Figure 7). In this frame, the specific requirement of Cdc7 during the S phase would be a response to DNA damage to maintain the interactions and assist stressed forks.

How the MCM/Rad51 interaction promotes replicative and repair functions and whether they are mechanistically related is unknown. They seem to occur through non-recombinogenic mechanisms, which points to TLS. This might explain the mild sensitivity to MMS of both *rad51m* and, more specifically, *rad51-C159R*. One possibility is that these physical interactions provide a platform for the landing of replication and repair factors at the proximity of stressed forks. Recently, we showed that Rad51 and Rad52 have a non-recombinogenic role in TLS by facilitating the recruitment of the Rad6/Rad18 complex to chromatin (Cano-Linares et al., 2021). Proliferating cell nuclear antigen (PCNA) ubiquitylation by Rad6/Rad18 is necessary for the recruitment of TLS polymerases (Bienko et al., 2005) and facilitates replication fork advance in the presence of a damaged template (Ortiz-Bazán et al., 2014). In this frame, the MCM/Rad51 interaction might speed up DNA synthesis in the presence of blocking lesions by promoting TLS at the fork. Whether the MCM/Rad51 interaction promotes the recruitment of these and/or additional repair/replication factors or operates through different mechanisms will require further studies.

In sum, a DDT mechanism has evolved in yeast cells that relies on the accumulation of MCM/Rad51/Rad52 complexes in a nucleoprotein scaffold before replication firing to facilitate the assistance to stressed replication forks. Physical interactions of MCM with Rad51 and Rad52 are also detected in mammalian cells (Bailis et al., 2008; Shukla et al., 2005). Therefore, they seem to have a conserved role whose study may help provide an understanding about how cells deal with replicative stress.

STAR★METHODS

Detailed methods are provided in the online version of this paper and include the following:

- KEY RESOURCES TABLE
- RESOURCE AVAILABILITY
  - Lead contact
  - Materials availability
  - Data and code availability
- EXPERIMENTAL MODEL AND SUBJECT DETAILS
- METHOD DETAILS
  - Plasmids
  - Growth conditions
  - Search for rad51 mutants
  - DNA damage sensitivity and cell viability
  - Genetic recombination
  - DNA repair foci analysis
  - Flow cytometry and budding analyses
  - Pulse field gel electrophoresis (PFGE)
  - DNA fiber assay
  - 2D-gel electrophoresis
  - *In vivo* ChEC analyses
  - Chromatin immunoprecipitation analysis
  - Fractionation analyses
  - Coimmunoprecipitation
  - Western blot
- QUANTIFICATION AND STATISTICAL ANALYSIS
  - Image processing and analysis
  - Statistical analyses

SUPPLEMENTAL INFORMATION

Supplemental information can be found online at https://doi.org/10.1016/j.celrep.2021.109440.

ACKNOWLEDGMENTS

We thank Gislene Pereira, Heinrich Leonhardt, Philippe Pasero, Nancy M. Hollingsworth, Michael T. Fasullo, Hiroshi Masumoto, and Lorraine Symington for various strains and reagents and Pedro San Segundo, Felipe Cortes Ledesma, and Fernando Monje Casas for critical reading of the manuscript. This work was supported by grants BFU2015-63698-P and PGC2018-099182-B-I00 (to F.P.) from the Spanish government, and project-ID 393547839-SFB1361 (to H.D.U.) from the Deutsche Forschungsgemeinschaft (DFG, German Research Foundation). M.J.C.-L., M.I.C.-L., C.G.-G, A.Y.-V., and R.G.-P were recipients of pre-doctoral training grants from the Spanish government.

AUTHOR CONTRIBUTIONS

Investigation, M.J.C.-L., C.G.-G., M.I.C.-L., R.P.W., A.Y.-V., M.M.-H., J.M.R.-R., M.V., and R.G.-P.; conceptualization, F.P.; writing – original draft, F.P.; writing – review & editing, F.P. and H.D.U.; funding acquisition, F.P. and H.D.U.

DECLARATION OF INTERESTS

The authors declare no competing interests.

Received: November 24, 2020
Revised: May 28, 2021
Accepted: July 1, 2021
Published: July 27, 2021

SUPPORTING CITATIONS

The following references appear in the Supplemental information: Gallego-Sánchez et al. (2012); Ogi et al. (2008).

REFERENCES

Alabert, C., Bianco, J.N., and Pasero, P. (2009). Differential regulation of homologous recombination at DNA breaks and replication forks by the Mrc1 branch of the S-phase checkpoint. EMBO J. *28*, 1131–1141.

Alabert, C., Bukowski-Wills, J.-C., Lee, S.-B., Kustatscher, G., Nakamura, K., de Lima Alves, F., Menard, P., Mejlvang, J., Rappsilber, J., and Groth, A. (2014). Nascent chromatin capture proteomics determines chromatin dynamics during DNA replication and identifies unknown fork components. Nat. Cell Biol. *16*, 281–293.

Alvaro, D., Sunjevaric, I., Reid, R.J.D., Lisby, M., Stillman, D.J., and Rothstein, R. (2006). Systematic hybrid LOH: a new method to reduce false positives and negatives during screening of yeast gene deletion libraries. Yeast *23*, 1097–1106.

Aparicio, O.M., Weinstein, D.M., and Bell, S.P. (1997). Components and dynamics of DNA replication complexes in *S. cerevisiae*: redistribution of MCM proteins and Cdc45p during S phase. Cell *91*, 59–69.

Bailis, J.M., Luche, D.D., Hunter, T., and Forsburg, S.L. (2008). Minichromosome maintenance proteins interact with checkpoint and recombination proteins to promote s-phase genome stability. Mol. Cell. Biol. *28*, 1724–1738.

Barlow, J.H., and Rothstein, R. (2009). Rad52 recruitment is DNA replication independent and regulated by Cdc28 and the Mec1 kinase. EMBO J. *28*, 1121–1130.

Bastia, D., Srivastava, P., Zaman, S., Choudhury, M., Mohanty, B.K., Bacal, J., Langston, L.D., Pasero, P., and O'Donnell, M.E. (2016). Phosphorylation of CMG helicase and Tof1 is required for programmed fork arrest. Proc. Natl. Acad. Sci. USA *113*, E3639–E3648.

Bertazzi, D.T., Kurtulmus, B., and Pereira, G. (2011). The cortical protein Lte1 promotes mitotic exit by inhibiting the spindle position checkpoint kinase Kin4. J. Cell Biol. *193*, 1033–1048.

Bhat, K.P., and Cortez, D. (2018). RPA and RAD51: fork reversal, fork protection, and genome stability. Nat. Struct. Mol. Biol. *25*, 446–453.

Bienko, M., Green, C.M., Crosetto, N., Rudolf, F., Zapart, G., Coull, B., Kannouche, P., Wider, G., Peter, M., Lehmann, A.R., et al. (2005). Ubiquitin-binding domains in Y-family polymerases regulate translesion synthesis. Science *310*, 1821–1824.

Branzei, D., and Foiani, M. (2010). Maintaining genome stability at the replication fork. Nat. Rev. Mol. Cell Biol. *11*, 208–219.

Branzei, D., and Psakhye, I. (2016). DNA damage tolerance. Curr. Opin. Cell Biol. *40*, 137–144.

Branzei, D., Vanoli, F., and Foiani, M. (2008). SUMOylation regulates Rad18-mediated template switch. Nature *456*, 915–920.

Braun, K.A., and Breeden, L.L. (2007). Nascent transcription of MCM2-7 is important for nuclear localization of the minichromosome maintenance complex in G1. Mol. Biol. Cell *18*, 1447–1456.

Bruck, I., and Kaplan, D.L. (2015). Conserved mechanism for coordinating replication fork helicase assembly with phosphorylation of the helicase. Proc. Natl. Acad. Sci. USA *112*, 11223–11228.

Cano-Linares, M.I., Yáñez-Vilches, A., García-Rodríguez, N., Barrientos-Moreno, M., González-Prieto, R., San-Segundo, P., Ulrich, H.D., and Prado, F. (2021). Non-recombinogenic roles for Rad52 in translesion synthesis during DNA damage tolerance. EMBO Rep. *22*, e50410.

Clemente-Ruiz, M., and Prado, F. (2009). Chromatin assembly controls replication fork stability. EMBO Rep. *10*, 790–796.

Cocker, J.H., Piatti, S., Santocanale, C., Nasmyth, K., and Diffley, J.F. (1996). An essential role for the Cdc6 protein in forming the pre-replicative complexes of budding yeast. Nature *379*, 180–182.

Das, S.P., and Rhind, N. (2016). How and why multiple MCMs are loaded at origins of DNA replication. BioEssays *38*, 613–617.

Das, S.P., Borrman, T., Liu, V.W.T., Yang, S.C.-H., Bechhoefer, J., and Rhind, N. (2015). Replication timing is regulated by the number of MCMs loaded at origins. Genome Res. *25*, 1886–1892.

Deegan, T.D., and Diffley, J.F.X. (2016). MCM: one ring to rule them all. Curr. Opin. Struct. Biol. *37*, 145–151.

Donovan, S., Harwood, J., Drury, L.S., and Diffley, J.F. (1997). Cdc6p-dependent loading of Mcm proteins onto pre-replicative chromatin in budding yeast. Proc. Natl. Acad. Sci. USA *94*, 5611–5616.

Fasullo, M.T., and Davis, R.W. (1987). Recombinational substrates designed to study recombination between unique and repetitive sequences in vivo. Proc. Natl. Acad. Sci. USA *84*, 6215–6219.

Feser, J., Truong, D., Das, C., Carson, J.J., Kieft, J., Harkness, T., and Tyler, J.K. (2010). Elevated histone expression promotes life span extension. Mol. Cell *39*, 724–735.

Foiani, M., Marini, F., Gamba, D., Lucchini, G., and Plevani, P. (1994). The B subunit of the DNA polymerase alpha-primase complex in *Saccharomyces cerevisiae* executes an essential function at the initial stage of DNA replication. Mol. Cell. Biol. *14*, 923–933.

Frei, C., and Gasser, S.M. (2000). The yeast Sgs1p helicase acts upstream of Rad53p in the DNA replication checkpoint and colocalizes with Rad53p in S-phase-specific foci. Genes Dev. *14*, 81–96.

Fung, C.W., Fortin, G.S., Peterson, S.E., and Symington, L.S. (2006). The rad51-K191R ATPase-defective mutant is impaired for presynaptic filament formation. Mol. Cell. Biol. *26*, 9544–9554.

Gallego-Sánchez, A., Andrés, S., Conde, F., San-Segundo, P.A., and Bueno, A. (2012). Reversal of PCNA ubiquitylation by Ubp10 in *Saccharomyces cerevisiae*. PLoS Genet. *8*, e1002826.

Gangavarapu, V., Prakash, S., and Prakash, L. (2007). Requirement of RAD52 group genes for postreplication repair of UV-damaged DNA in *Saccharomyces cerevisiae*. Mol. Cell. Biol. *27*, 7758–7764.

Ge, X.Q., Jackson, D.A., and Blow, J.J. (2007). Dormant origins licensed by excess Mcm2-7 are required for human cells to survive replicative stress. Genes Dev. *21*, 3331–3341.

Giannattasio, M., Zwicky, K., Follonier, C., Foiani, M., Lopes, M., and Branzei, D. (2014). Visualization of recombination-mediated damage bypass by template switching. Nat. Struct. Mol. Biol. *21*, 884–892.

González-Prieto, R., Muñoz-Cabello, A.M., Cabello-Lobato, M.J., and Prado, F. (2013). Rad51 replication fork recruitment is required for DNA damage tolerance. EMBO J. *32*, 1307–1321.

González-Prieto, R., Cabello-Lobato, M.J., and Prado, F. (2021). In vivo binding of recombination proteins to non-DSB DNA lesions and to replication forks. Methods Mol. Biol. *2153*, 447–458.

Hardy, C.F., Dryga, O., Seematter, S., Pahl, P.M., and Sclafani, R.A. (1997). mcm5/cdc46-bob1 bypasses the requirement for the S phase activator Cdc7p. Proc. Natl. Acad. Sci. USA *94*, 3151–3155.

Hashimoto, Y., Ray Chaudhuri, A., Lopes, M., and Costanzo, V. (2010). Rad51 protects nascent DNA from Mre11-dependent degradation and promotes continuous DNA synthesis. Nat. Struct. Mol. Biol. *17*, 1305–1311.

Hecht, A., and Grunstein, M. (1999). Mapping DNA interaction sites of chromosomal proteins using immunoprecipitation and polymerase chain reaction. Methods Enzymol. *304*, 399–414.

Hesketh, E.L., Knight, J.R.P., Wilson, R.H.C., Chong, J.P.J., and Coverley, D. (2015). Transient association of MCM complex proteins with the nuclear matrix during initiation of mammalian DNA replication. Cell Cycle *14*, 333–341.

Heyer, W.-D., Ehmsen, K.T., and Liu, J. (2010). Regulation of homologous recombination in eukaryotes. Annu. Rev. Genet. *44*, 113–139.

Hills, S.A., and Diffley, J.F.X. (2014). DNA replication and oncogene-induced replicative stress. Curr. Biol. *24*, R435–R444.

Hoang, M.L., Leon, R.P., Pessoa-Brandao, L., Hunt, S., Raghuraman, M.K., Fangman, W.L., Brewer, B.J., and Sclafani, R.A. (2007). Structural changes in Mcm5 protein bypass Cdc7-Dbf4 function and reduce replication origin efficiency in *Saccharomyces cerevisiae*. Mol. Cell. Biol. *27*, 7594–7602.

Hyrien, O. (2016). How MCM loading and spreading specify eukaryotic DNA replication initiation sites. F1000Res. *5*, 2063.

Ibarra, A., Schwob, E., and Méndez, J. (2008). Excess MCM proteins protect human cells from replicative stress by licensing backup origins of replication. Proc. Natl. Acad. Sci. USA *105*, 8956–8961.

Jachymczyk, W.J., Chlebowicz, E., Swietlinska, Z., and Zuk, J. (1977). Alkaline sucrose sedimentation studies of MMS-induced DNA single-strand breakage and rejoining in the wild type and in UV-sensitive mutants of *Saccharomyces cerevisiae*. Mutat. Res. *43*, 1–10.

Kilic, S., Lezaja, A., Gatti, M., Bianco, E., Michelena, J., Imhof, R., and Altmeyer, M. (2019). Phase separation of 53BP1 determines liquid-like behavior of DNA repair compartments. EMBO J. *38*, e101379.

Labib, K. (2010). How do Cdc7 and cyclin-dependent kinases trigger the initiation of chromosome replication in eukaryotic cells? Genes Dev. *24*, 1208–1219.

Li, H., and O'Donnell, M.E. (2018). The eukaryotic CMG helicase at the replication fork: emerging architecture reveals an unexpected mechanism. BioEssays *40*, 1700208–1700209.

Li, X., Zhang, X.-P., Solinger, J.A., Kiianitsa, K., Yu, X., Egelman, E.H., and Heyer, W.-D. (2007). Rad51 and Rad54 ATPase activities are both required

to modulate Rad51-dsDNA filament dynamics. Nucleic Acids Res. *35*, 4124–4140.

Liang, C., and Stillman, B. (1997). Persistent initiation of DNA replication and chromatin-bound MCM proteins during the cell cycle in cdc6 mutants. Genes Dev. *11*, 3375–3386.

Liberi, G., Maffioletti, G., Lucca, C., Chiolo, I., Baryshnikova, A., Cotta-Ramusino, C., Lopes, M., Pellicioli, A., Haber, J.E., and Foiani, M. (2005). Rad51-dependent DNA structures accumulate at damaged replication forks in sgs1 mutants defective in the yeast ortholog of BLM RecQ helicase. Genes Dev. *19*, 339–350.

Lisby, M., Rothstein, R., and Mortensen, U.H. (2001). Rad52 forms DNA repair and recombination centers during S phase. Proc. Natl. Acad. Sci. USA *98*, 8276–8282.

Longtine, M.S., III, McKenzie, A., III, Demarini, D.J., Shah, N.G., Wach, A., Brachat, A., Philippsen, P., and Pringle, J.R. (1998). Additional modules for versatile and economical PCR-based gene deletion and modification in *Saccharomyces cerevisiae*. Yeast *14*, 953–961.

Lopes, M., Foiani, M., and Sogo, J.M. (2006). Multiple mechanisms control chromosome integrity after replication fork uncoupling and restart at irreparable UV lesions. Mol. Cell *21*, 15–27.

López-Contreras, A.J., Ruppen, I., Nieto-Soler, M., Murga, M., Rodriguez-Acebes, S., Remeseiro, S., Rodrigo-Perez, S., Rojas, A.M., Méndez, J., Muñoz, J., and Fernandez-Capetillo, O. (2013). A proteomic characterization of factors enriched at nascent DNA molecules. Cell Rep. *3*, 1105–1116.

Lord, S.J., Velle, K.B., Mullins, R.D., and Fritz-Laylin, L.K. (2020). SuperPlots: communicating reproducibility and variability in cell biology. J. Cell Biol. *219*, e202001064.

Lundin, C., North, M., Erixon, K., Walters, K., Jenssen, D., Goldman, A.S.H., and Helleday, T. (2005). Methyl methanesulfonate (MMS) produces heat-labile DNA damage but no detectable in vivo DNA double-strand breaks. Nucleic Acids Res. *33*, 3799–3811.

Maki, K., Inoue, T., Onaka, A., Hashizume, H., Somete, N., Kobayashi, Y., Murakami, S., Shigaki, C., Takahashi, T.S., Masukata, H., and Nakagawa, T. (2011). Abundance of prereplicative complexes (Pre-RCs) facilitates recombinational repair under replication stress in fission yeast. J. Biol. Chem. *286*, 41701–41710.

Mankouri, H.W., Ngo, H.-P., and Hickson, I.D. (2007). Shu proteins promote the formation of homologous recombination intermediates that are processed by Sgs1-Rmi1-Top3. Mol. Biol. Cell *18*, 4062–4073.

McCullum, E.O., Williams, B.A.R., Zhang, J., and Chaput, J.C. (2010). Random mutagenesis by error-prone PCR. Methods Mol. Biol. *634*, 103–109.

Miné-Hattab, J., Heltberg, M., Villemeur, M., Guedj, C., Mora, T., Walczak, A.M., Dahan, M., and Taddei, A. (2021). Single molecule microscopy reveals key physical features of repair foci in living cells. eLife *10*, e60577.

Morgan, E.A., Shah, N., and Symington, L.S. (2002). The requirement for ATP hydrolysis by *Saccharomyces cerevisiae* Rad51 is bypassed by mating-type heterozygosity or RAD54 in high copy. Mol. Cell. Biol. *22*, 6336–6343.

Mortensen, U.H., Bendixen, C., Sunjevaric, I., and Rothstein, R. (1996). DNA strand annealing is promoted by the yeast Rad52 protein. Proc. Natl. Acad. Sci. USA *93*, 10729–10734.

Naumov, G.I., Naumova, E.S., Lantto, R.A., Louis, E.J., and Korhola, M. (1992). Genetic homology between *Saccharomyces cerevisiae* and its sibling species S. paradoxus and S. bayanus: electrophoretic karyotypes. Yeast *8*, 599–612.

Nguyen, V.Q., Co, C., and Li, J.J. (2001). Cyclin-dependent kinases prevent DNA re-replication through multiple mechanisms. Nature *411*, 1068–1073.

Ogi, H., Wang, C.-Z., Nakai, W., Kawasaki, Y., and Masumoto, H. (2008). The role of the *Saccharomyces cerevisiae* Cdc7-Dbf4 complex in the replication checkpoint. Gene *414*, 32–40.

Ortiz-Bazán, M.Á., Gallo-Fernández, M., Saugar, I., Jiménez-Martín, A., Vázquez, M.V., and Tercero, J.A. (2014). Rad5 plays a major role in the cellular response to DNA damage during chromosome replication. Cell Rep. *9*, 460–468.

Pasero, P., Duncker, B.P., Schwob, E., and Gasser, S.M. (1999). A role for the Cdc7 kinase regulatory subunit Dbf4p in the formation of initiation-competent origins of replication. Genes Dev. *13*, 2159–2176.

Prado, F. (2014). Homologous recombination maintenance of genome integrity during DNA damage tolerance. Mol. Cell. Oncol. *1*, e957039.

Prado, F. (2018). Homologous recombination: to fork and beyond. Genes (Basel) *9*, 603.

Prado, F., and Aguilera, A. (1995). Role of reciprocal exchange, one-ended invasion crossover and single-strand annealing on inverted and direct repeat recombination in yeast: different requirements for the RAD1, RAD10, and RAD52 genes. Genetics *139*, 109–123.

Prado, F., and Aguilera, A. (2005). Partial depletion of histone H4 increases homologous recombination-mediated genetic instability. Mol. Cell. Biol. *25*, 1526–1536.

Prakash, L. (1981). Characterization of postreplication repair in *Saccharomyces cerevisiae* and effects of rad6, rad18, rev3 and rad52 mutations. Mol. Gen. Genet. *184*, 471–478.

Resnick, M.A., Boyce, J., and Cox, B. (1981). Postreplication repair in *Saccharomyces cerevisiae*. J. Bacteriol. *146*, 285–290.

Rothbauer, U., Zolghadr, K., Tillib, S., Nowak, D., Schermelleh, L., Gahl, A., Backmann, N., Conrath, K., Muyldermans, S., Cardoso, M.C., and Leonhardt, H. (2006). Targeting and tracing antigens in live cells with fluorescent nanobodies. Nat. Methods *3*, 887–889.

Rothbauer, U., Zolghadr, K., Muyldermans, S., Schepers, A., Cardoso, M.C., and Leonhardt, H. (2008). A versatile nanotrap for biochemical and functional studies with fluorescent fusion proteins. Mol. Cell. Proteomics *7*, 282–289.

Schmid, M., Durussel, T., and Laemmli, U.K. (2004). ChIC and ChEC: genomic mapping of chromatin proteins. Mol. Cell *16*, 147–157.

Shah, P.P., Zheng, X., Epshtein, A., Carey, J.N., Bishop, D.K., and Klein, H.L. (2010). Swi2/Snf2-related translocases prevent accumulation of toxic Rad51 complexes during mitotic growth. Mol. Cell *39*, 862–872.

Sheff, M.A., and Thorn, K.S. (2004). Optimized cassettes for fluorescent protein tagging in *Saccharomyces cerevisiae*. Yeast *21*, 661–670.

Shukla, A., Navadgi, V.M., Mallikarjuna, K., and Rao, B.J. (2005). Interaction of hRad51 and hRad52 with MCM complex: a cross-talk between recombination and replication proteins. Biochem. Biophys. Res. Commun. *329*, 1240–1245.

Sikorski, R.S., and Hieter, P. (1989). A system of shuttle vectors and yeast host strains designed for efficient manipulation of DNA in *Saccharomyces cerevisiae*. Genetics *122*, 19–27.

Sung, P., and Stratton, S.A. (1996). Yeast Rad51 recombinase mediates polar DNA strand exchange in the absence of ATP hydrolysis. J. Biol. Chem. *271*, 27983–27986.

Tanaka, T., Knapp, D., and Nasmyth, K. (1997). Loading of an Mcm protein onto DNA replication origins is regulated by Cdc6p and CDKs. Cell *90*, 649–660.

Van Komen, S., Petukhova, G., Sigurdsson, S., Stratton, S., and Sung, P. (2000). Superhelicity-driven homologous DNA pairing by yeast recombination factors Rad51 and Rad54. Mol. Cell *6*, 563–572.

Vanoli, F., Fumasoni, M., Szakal, B., Maloisel, L., and Branzei, D. (2010). Replication and recombination factors contributing to recombination-dependent bypass of DNA lesions by template switch. PLoS Genet. *6*, e1001205.

Vázquez, M.V., Rojas, V., and Tercero, J.A. (2008). Multiple pathways cooperate to facilitate DNA replication fork progression through alkylated DNA. DNA Repair (Amst.) *7*, 1693–1704.

Wan, L., Zhang, C., Shokat, K.M., and Hollingsworth, N.M. (2006). Chemical inactivation of cdc7 kinase in budding yeast results in a reversible arrest that allows efficient cell synchronization prior to meiotic recombination. Genetics *174*, 1767–1774.

Waterman, D.P., Zhou, F., Li, K., Lee, C.-S., Tsabar, M., Eapen, V.V., Mazzella, A., and Haber, J.E. (2019). Live cell monitoring of double strand breaks in *S. cerevisiae*. PLoS Genet. *15*, e1008001–e1008022.

Weinreich, M., and Stillman, B. (1999). Cdc7p-Dbf4p kinase binds to chromatin during S phase and is regulated by both the APC and the RAD53 checkpoint pathway. EMBO J. *18*, 5334–5346.

Wilson, R.H.C., and Coverley, D. (2013). Relationship between DNA replication and the nuclear matrix. Genes Cells *18*, 17–31.

Wong, R.P., García-Rodríguez, N., Zilio, N., Hanulová, M., and Ulrich, H.D. (2020). Processing of DNA polymerase-blocking lesions during genome replication is spatially and temporally segregated from replication forks. Mol. Cell *77*, 3–16.e4.

Wyrick, J.J., Aparicio, J.G., Chen, T., Barnett, J.D., Jennings, E.G., Young, R.A., Bell, S.P., and Aparicio, O.M. (2001). Genome-wide distribution of ORC and MCM proteins in *S. cerevisiae*: high-resolution mapping of replication origins. Science *294*, 2357–2360.

Zellweger, R., Dalcher, D., Mutreja, K., Berti, M., Schmid, J.A., Herrador, R., Vindigni, A., and Lopes, M. (2015). Rad51-mediated replication fork reversal is a global response to genotoxic treatments in human cells. J. Cell Biol. *208*, 563–579.

STAR★METHODS

KEY RESOURCES TABLE

REAGENT or RESOURCE	SOURCE	IDENTIFIER
Antibodies		
Mouse monoclonal anti GFP	Clontech	Cat# 632381
Rabbit polyclonal anti-Rad51	Santa Cruz	Cat# sc-33626
Rabbit polyclonal anti-Rad51	Abcam (= Antibodies.com)	Cat# ab63798 (= A284)
Rat monoclonal anti-HA	Roche	Cat# 11867423001 (3F10)
Mouse monoclonal anti-HA	Roche	Cat# 11666606001 (12CA5)
Goat polyclonal anti-Mcm7	Santa Cruz	Cat# sc-6688
Mouse monoclonal anti-Mcm4	Santa Cruz	Cat# sc-166036
Rabbit polyclonal anti-Rad52	(Mortensen et al., 1996)	N/A
Mouse monoclonal anti-Pgk1	Invitrogen	Cat# 22C5D8
Rabbit polyclonal anti-H4	Abcam	Cat# ab10158
Rat monoclonal anti-BrdU	Abcam	Cat# ab6326
Mouse monoclonal anti-single stranded DNA	Sigma-Aldrich	Cat# MAB3034
Goat anti-rat Cy5	Abcam	Cat# ab6565
Goat anti-mouse Cy3	Abcam	Cat# ab6946
Chemicals, peptides, and recombinant proteins		
Methyl-methanesulfonate (MMS)	Merck	Cat# 129925-256
Hydroxyurea (HU)	Material Blanco de Laboratorio, S.L.	Cat# H9120
α-factor	AB BCN S.L.	N/A
α-factor	Proteogenix SAS	Cat# GM-PT301350-95
Pronase	Merck	Cat# 10165921001
Nocodazole	Merck	Cat# M1404-50MG
PP1 Analog II (1NMPP1)	Merck	Cat# 529581-1
PP1 Analog II (1NMPP1)	Santa Cruz	Cat# sc-203214
MNase I	Merck	Cat# N3755-200UN
benzonase	Merck	Cat# 70746-4
5-Bromo-2′-deoxyuridine (BrdU)	Sigma	Cat# B5002
Agarose, NuSieve GTG Agarose (low-melting temp)	Lonza	Cat# 50081
λ phosphatase	New England Biolabs	Cat# P0753S
Critical commercial assays		
GFP trap magnetic beads	Chromotek	Cat# gtma-100
dynabeads protein G	Invitrogen	Cat# 10004D
QuickChange XL Site-directed Mutagenesis Kit	Agilent	Cat# 200517
Experimental models: Organisms/strains		
S. cerevisiae: Strain background: W303	ATCC	ATTC: 208353
Other yeast strains: Table S1	This study	N/A
Oligonucleotides		
See Table S2	This study	N/A
Recombinant DNA		
pRS551-L120A,V181A	A gift from Nancy M. Hollingsworth, Stony Brook University	N/A
pRS51s	A gift from Andrés Aguilera, Seville University	N/A

(*Continued on next page*)

Continued

REAGENT or RESOURCE	SOURCE	IDENTIFIER
pRSRAD51g	This study	N/A
pRS313-51.54	This study	N/A
pRS306-r51.54	This study	N/A
p313r51-C159R	This study	N/A
pWJ1213	(Alvaro et al., 2006)	N/A
pWJ1344	(Alvaro et al., 2006)	N/A
pFA6a-MN-HIS3MX6	(Schmid et al., 2004)	N/A
pKT209	(Sheff and Thorn, 2004)	N/A
pFA6A-3HA- HIS3MX6	(Longtine et al., 1998)	N/A
pFA6a-GBP-KanMX4 (pHA29)	(Bertazzi et al., 2011; Rothbauer et al., 2006, 2008)	N/A
Software and algorithms		
Image Lab™	Biorad	http://www.bio-rad.com/es-es/product/image-lab-software?ID=KRE6P5E8Z
ImageGauge	Fujifilm	https://www.bioz.com/result/sciencelab98imagegaugesoftware/product/FUJIFILM
ImageJ	Fiji	https://imagej.net/software/fiji/
Prism	GraphPad	https://www.graphpad.com/scientific-software/prism/
Scatter SuperPlots	(Lord et al., 2020)	N/A

RESOURCE AVAILABILITY

Lead contact

Further information and requests for resources and reagents should be directed to and will be fulfilled by the lead contact, Félix Prado (felix.prado@cabimer.es)

Materials availability

All unique/stable reagents generated in this study are available from the Lead Contact without restriction.

Data and code availability

- All data reported in this paper will be shared by the lead contact upon request.
- This paper does not report original code.
- Any additional information required to reanalyze the data reported in this paper is available from the lead contact upon request.

EXPERIMENTAL MODEL AND SUBJECT DETAILS

Yeast strains used in this study are listed in Table S1. Tagged and deletion strains were constructed by a PCR-based strategy (Longtine et al., 1998). The uSCE system was backcrossed five times into the W303 background (Cano-Linares et al., 2021). The integrative plasmids pRS551-L120A,V181A (a gift from N. Hollingsworth) and pRS306-r51.54 (see Method details) were used to replace *CDC7* and *RAD51* with *cdc7-as3* (W303cdc7as3-2) and *rad51m* (w303.51.54-7), respectively. Briefly, a wild-type strain was transformed with either pRS551-L120A,V181A or pRS306-r51.54 (cut with EcoRI) and grown first in medium without uracil to select the integration event (that duplicates the gene) and then in medium with 5-fluoroorotic acid to select strains that had lost one of the two copies and the intervening sequence. *cdc7-as3* and *rad51m* strains were selected by 1NMPP1-dependent cell growth inhibition and MMS sensitivity, respectively, and confirmed by DNA sequencing.

METHOD DETAILS

Plasmids

pWJ1213 and pWJ1344 are a centromeric plasmid expressing *RAD52-YFP* (Alvaro et al., 2006). pFA6a-MN-HIS3MX6 (Schmid et al., 2004), pKT209 (Sheff and Thorn, 2004), pFA6A-3HA- HIS3MX6 (Longtine et al., 1998) and pHA29 (pFA6a-GBP-KanMX4)

(Bertazzi et al., 2011; Rothbauer et al., 2006, 2008) are plasmids for protein tagging with MNaseI, eGFP, HA and GBP, respectively. pRS551-L120A,V181A (a gift from N. Hollingsworth) is an integrative plasmid to replace *CDC7* with *cdc7-as3*. pRSRAD51g and pRS51s are centromeric plasmids expressing *RAD51* and either *URA3* or *HIS3*, respectively. pRSRAD51g was constructed by inserting a 2.4 kb PCR fragment containing the *RAD51* allele at the BamHI-HindIII site of pRS316 (Sikorski and Hieter, 1989). pRSR51s (A. Aguilera's lab) was constructed by inserting the genomic *Eco*RV-BamHI fragment containing the *RAD51* allele at the *Eco*RV-BamHI site of pRS313 (Sikorski and Hieter, 1989). pRS313-51.54 is identical to pRSR51s but it contains the *rad51m* allele (see Search for rad51 mutants). pRS306-r51.54 is an integrative plasmid containing the *rad51m* allele. It was constructed by inserting the BamHI-HindIII fragment from pRS313-r51.54 (containing *rad51m*) at the BamHI-HindIII site of pRS306 (Sikorski and Hieter, 1989). The p313r51-C159R plasmid was generated by directed mutagenesis of the *RAD51* gene in the pRSR51s plasmid with the QuickChange XL Site-Directed Mutagenesis Kit (200517; Agilent).

Growth conditions

Yeast cells were grown at 30°C in supplemented minimal medium (SMM), except for experiments that required synchronization in metaphase, which were performed in YPAD rich medium with 15 μg/ml nocodazole for 1 h. For G1 synchronization, cells were grown to mid-log phase and α-factor was added twice at 60 min intervals at either 2 (*BAR1* strains) or 0.25 μg/ml (*bar1Δ* strains). Then, cells were washed three times and released into fresh medium with 50 μg/ml pronase (to remove α-factor) in the absence or presence of MMS at the indicated concentrations. To eliminate the MMS before releasing cells into fresh medium, samples were treated with 2.5% sodium thiosulfate to inactivate it and then washed three times. For Cdc6 depletion, *GAL::CDC6* cells were synchronized in G1 with α-factor, released into fresh medium with 1% DMSO and 15 μg/ml nocodazole for 90 min to arrest in metaphase, incubated with 2% glucose and fresh nocodazole for 1 h, and released with 2% glucose and α-factor for 2.5 h.

Search for rad51 mutants

An *in vivo* library enriched in *rad51* mutants was constructed by co-transforming a *rad51Δ* strain containing pRSRAD51g (centromeric plasmid expressing the *RAD51* and *URA3* genes) with 1) the plasmid pRS51s (centromeric plasmid expressing the *RAD51* and *HIS3* genes) linearized at the *RAD51* ORF with EcoRI and 2) a mutagenic PCR product of *RAD51* (McCullum et al., 2010). Cells were plated onto SMM – His to select transformants that recircularized pRS51s. Recircularization by HR with either the PCR product or pRSRAD51g was ~4 and ~20 times more efficient than recircularization by HR with just pRSRAD51g or recircularization by NHEJ (estimated in a *rad51Δ* strain containing pRS316 instead of pRSRAD51g). Next, transformants were replica-plated onto SMM medium containing 5′-fluoroorotic acid to select for cells that had lost pRSRAD51g. This strategy restricts the expression of *RAD51* to the *in vivo* cloning and allows the screening of *rad51* mutants. To search for mutants sensitive to MMS and resistance to IR, cells were either grown onto SMM medium at different MMS concentrations or plated onto SMM medium, irradiated at different doses and then grown under unperturbed conditions. Plasmids from positive clones were isolated; the phenotype was confirmed with new *rad51Δ* transformants and the mutations determined by DNA sequencing of the plasmids.

DNA damage sensitivity and cell viability

MMS sensitivity was determined by spotting ten-fold serial dilutions of the same number of mid-log growing cells onto medium with or without the drug (chronic damage). For IR sensitivity spotted cells were irradiated and then grown under unperturbed conditions (acute damage). Cell viability was determined from exponentially growing cultures treated either with MMS or IR as the frequency of cells able to form colonies after DNA damage relative to untreated cells, taken as 100.

Genetic recombination

HR was determined by measuring the frequency of His+ recombinants generated by uSCE in a chromosomal-integrated system (Fasullo and Davis, 1987). Recombination frequencies were determined by fluctuation tests as previously reported (Prado and Aguilera, 1995) but from liquid cultures. Briefly, six independent cell cultures (started with a colony) were grown to the same mid-log phase and then treated with different concentrations of MMS for 4 hours or irradiated with IR at different doses. Cells form untreated and treated cultures were plated with the appropriate dilutions onto SMM without histidine and SMM to calculate recombinants and total viable cells (as colony-forming units), respectively. The frequency of HR was calculated using the median of recombinants and the mean of total cells. To have a more accurate value, the mean and SEM of at least 3 independent fluctuation tests are given.

DNA repair foci analysis

The percentage of cells with Rad52 or RPA foci was determined as described previously (Lisby et al., 2001). Cells expressing Rfa1-YFP or transformed with plasmid pWJ1344 or pWJ1213 (expressing Rad52-YFP) were grown in liquid culture under the indicated conditions, fixed with 2.5% formaldehyde in 0.1M potassium phosphate pH 6.4 for 10 minutes, washed twice with 0.1M potassium phosphate pH 6.6 and resuspended in 0.1M potassium phosphate pH 7.4. Finally, cells were fixed with 80% ethanol for 10 minutes, resuspended in H_2O or DAPI and visualized with a Leica CTR6000 fluorescence microscope. The percentage of cells with foci was counted directly on the processed samples under the microscope or on acquired images. In this case, six contrast and fluorescence images along the z axis (0.49 μm length each) were acquired with a CCD camera (Leica DFC350 FX) to find well-defined foci. Images

were processed and analyzed with the MetaMorph software (Molecular devices). A total number of approximately 100 cells were analyzed for each time point and experiment.

Flow cytometry and budding analyses

DNA content analysis was performed by flow cytometry as reported previously (Prado and Aguilera, 2005). Cells were fixed with 70% ethanol, washed with phosphate-buffered saline (PBS), incubated with 1 mg of RNaseA/ ml PBS, and stained with 5 μg/ml propidium iodide. Samples were sonicated to separate single cells and analyzed in a FACSCalibur flow cytometer. The percentage of budded cells was determined by counting 100 cells for each time point and experiment.

Pulse field gel electrophoresis (PFGE)

Replicating and complete chromosomes were resolved by PFGE (Biorad; 120o field angle; 6 V/cm; 14oC; initial block: switch time of 70 s for 16 h; final block: switch time of 120 s for 12 h). Total DNA from cultures growing at the indicated conditions was extracted in low-melting agarose (50081; Lonza) plugs as described (Naumov et al., 1992), but the incubation with Proteinase K was performed in buffer L (10 mM TrisHCl pH 8.0, 100 mM EDTA pH 8.0, 20 mM NaCl, SDS1%) at 30°C for 24 h to avoid heat-induced breakage of methylated DNA during sample preparation (Lundin et al., 2005). Gels were stained with ethidium bromide, and the signals were acquired in a Fuji FLA5100 and quantified with the ImageGauge software (Fujifilm).

DNA fiber assay

G1-synchronized cells were incubated with 0.4 mg/ml BrdU for 15 minutes, washed twice in water and released into fresh medium containing 0.4 mg/ml BrdU and 50 μg/ml pronase with or without 0.025% MMS. Cells were harvested at indicated time points to isolate genomic DNA for molecular combing. Briefly, yeast cells were spheroplasted with zymolyase to over 90% completion. 0.3×10^9 cells were embedded in low melting point agarose and incubated with 1 mg/ml Proteinase K in 125 mM EDTA pH9.5 containing 1% Sarkosyl for 2 days with one change of buffer in between. Plugs were washed thoroughly in TE buffer with 100 mM NaCl and once with 100 mM MES buffer pH6.0 and 100 mM NaCl. Plugs were melted in MES buffer with NaCl at 68 C for 15 minutes and digested overnight with Agarase (3 units per plug) at 45°C. Agarase was inactivated at 65 C for 10 minutes and the DNA solution was cooled down to room temperature. DNA fibers were combed on silanized coverslips (Combicoverslips, Genomic Vision) at a constant speed of 350 μm/s using DNA combing apparatus from Genomic Vision. Slides were baked at 65°C for at least 2 hours, denatured in 0.5M NaOH 1M NaCl for 15 minutes at room temperature and washed thrice in PBS. Slides were dehydrated in 70%, 90% and 100% EtOH and air-dried. For immunofluorescence staining, slides were blocked in BlockAid (Thermo Fisher Scientific) for 15 minutes at 37°C and incubated sequentially with 1:20 monoclonal rat anti-BrdU antibody (clone BU1/75; ab6326; Abcam), 1:50 monoclonal mouse anti-single stranded DNA antibody (clone 16-19; MAB3034; Sigma-Aldrich), and 1:100 goat anti-rat Cy5 (ab6565; Abcam) and goat anti-mouse Cy3 (ab6946; Abcam) secondary antibodies at 37°C for 1 hour with three PBS-T (1 × PBS with 0.1% Tween-20) washes in between each incubation. Slides were dehydrated in 70%, 90% and 100% and air-dried before mounting on Prolong Diamond mounting medium (Thermo Fisher Scientific). Images were obtained with the AF7000 widefield fluorescence microscope (Leica) equipped with a 63 × (NA = 1.4) oil immersion objective, ORCA-Flash 4.0 V2 digital CMOS camera (Hamamatsu), LED light source (SOLA, lumencor) and LAS AF software (Leica). Tile-scans were acquired with Z stacks of 4 planes with a step size of 0.2 μm. Cy3 signals were obtained with the N3 filter and Cy5 signals with the Y5 filter. Lengths of BrdU-labeled replication tracts were measured with ImageJ FIJI software. Inter-origin distances were calculated by measuring the distances between the middle point of each replication tract (replication origin) on the same fiber.

2D-gel electrophoresis

Replication intermediates were analyzed by 2D-gel electrophoresis from cells arrested with sodium azide (0.1% final concentration) and cooled down on ice as reported (Clemente-Ruiz and Prado, 2009). Briefly, total DNA was isolated with the G2/CTAB protocol, digested with *Eco*RV and *Hind*III, resolved by neutral/neutral two-dimensional gel electrophoresis, blotted to Hybond^{TM}-XL membranes, and analyzed by hybridization with an *ARS305* proximal ^{32}P-labeled probe (probe A). All signals were acquired in a Fuji FLA5100 and quantified with the ImageGauge software (Fujifilm).

In vivo ChEC analyses

Chromatin endogenous cleavage (ChEC) of Rad51-MN and Rad51m-MN cells was performed as reported (González-Prieto et al., 2013, 2021) from cultures grown in the presence or absence of MMS and arrested with sodium azide (0.1% final concentration). For cleavage induction, digitonin-permeabilized cells were incubated with 2 mM $CaCl_2$ at 30°C under gentle agitation. Total DNA was isolated and resolved into 0.8% TAE 1 × agarose gels. Gels were scanned in a Fuji FLA5100, and the signal profile quantified using the ImageGauge software (Fujifilm). The area of the DNA digestion profiles was equalized to eliminate DNA loading differences.

Chromatin immunoprecipitation analysis

Chromatin immunoprecipitation (ChIP) assays were performed as described (Hecht and Grunstein, 1999). Each sample was processed, split and incubated with antibodies either against GFP (632381, Clontech) or Rad51 (sc-33626, Santa Cruz or

ab63798, Abcam (= A284, Antibodies.com). Protein enrichment at each specific region was calculated as the ratio between the immunoprecipitated sample and the input in a *MCM4-GFP RAD51* strain relative to the same ratio in a *MCM4 rad51Δ* strain. Oligonucleotide sequences for the real-time PCR amplifications performed on purified DNA before (input) or after (immunoprecipitated) incubation with the antibodies are shown in Table S2.

Fractionation analyses

Fractionation was performed as described for chromatin fractionation in young yeast cells (Feser et al., 2010) with some modifications. Samples (15-30 ml) from mid-log phase cultures were collected by centrifugation, washed with cold 0.1mM Tris pH 9.4, 10mM DTT, and incubated for 15 min in 1 mL of the same buffer on ice. Cells were then washed with cold spheroplasting buffer (20mM HEPES pH 7.4, 1.2mM sorbitol, Roche Complete EDTA free protease inhibitor cocktail) and incubated with 1 mL of the same buffer with 210 μg zymoliase 20T for 1 h at 30°C. The spheroplasts were collected, washed twice with cold washing buffer (20mM Tris pH 7.4, 20mM KCl, 1M sorbitol, 0.1 μM spermine, 0.25 μM spermidine, protease inhibitors), and resuspended in 1 mL lysis buffer (20mM Tris pH 7.4, 20mM KCl, 0.4 M sorbitol, 0.1 μM spermine, 0.25 μM spermidine, 1% Triton X-100, protease inhibitors) for 5 min on ice. An aliquot (80 μl) was removed for the total sample, and the remaining sample was centrifuged for 15 min at 13000 g at 4°C to separate soluble (supernatant) and insoluble (pellet) fractions. Each pellet was washed with 0.5 mL cold lysis buffer and resuspended in 80 μL of water, and insoluble, soluble and total samples were mixed with SDS buffer for western blot analyses. Similar volumes were loaded for each time point for each kinetic, and similar cell equivalents of the insoluble and soluble fractions were loaded for the fractionation controls. To study nuclease-soluble and insoluble pellet fractions, the pellet generated after cell fractionation was resuspended in 100 μL of buffer (1mM Tris pH 7.4, 1mM MgCl2), incubated with 250 units of benzonase for 30 min at 37°C, and centrifuged 5 min at 13000 g. Similar volumes of soluble and non-soluble (resuspended in 100 μL of water) fractions were mixed with SDS buffer and loaded for western analyses.

Coimmunoprecipitation

CoIP was performed with 100-150 mL samples from mid-log phase cultures (O.D. ~0.75) that had been lysed with a Multi Beads Shocker (Yasui Kikai) at 4°C with 1x vol glass beads in 0.5 mL NP40 lysis buffer (50mM Tris pH 7.5, 150mM NaCl, 1% NP40) with protease inhibitors (1mM PMSF, 2mM DTT and Roche Complete EDTA free). Lysates were cleared by two consecutive centrifugation steps for 5 min at 1000 g (4°C) and, in case of nuclease treatment, mixed with MNaseI (15mM Tris, 50mM NaCl, 1.4mM $CaCl_2$, 0.2mM EDTA, 0.2mM EGTA pH 8.0) or benzonase buffer (50mM Tris pH 8.0, 1mM $MgCl_2$) and either 2.5 u MNaseI or 25 u benzonase and incubated for 20 min at 37°C. Samples were then collected by centrifugation for 15 min at 13000 g (4°C) and the total amount of protein at the supernatant was quantified by a Bradford assay. An aliquot of each sample was removed for the input. For GFP-based CoIPs, GFP trap magnetic beads (gtma-100; Chromotek) were incubated overnight at 4°C with similar amount of proteins (~12–16 mg) in NP40 lysis buffer, washed extensively with either standard (Mcm4-GFP CoIPs) or modified NP40 lysis buffer (50mM Tris pH 7.5, 500mM NaCl, 1% NP40) (Rad51-YFP CoIP). For the Mcm4-HA immunoprecipitation, samples were pre-cleared with dynabeads protein G (10004D, Invitrogen) during 2h at 4°C, and then incubated first with 0.5 μg/ml HA antibody high affinity (3F10, Roche; 11867423001) (overnight at 4°C) and then with dynabeads protein G (2h at 4°C), washed extensively with modified NP40 lysis buffer (50mM Tris pH 7.5, 1M NaCl, 1% NP40). Finally, samples were analyzed by western blot with the corresponding antibodies. Unless otherwise indicated, CoIP was performed with MNase I–treated lysates.

For CoIP from fractionated samples, chromatin and soluble fractions were prepared as above from 200 mL mid-log phase cultures except that spheroplasts were resuspended in 1 mL lysis buffer containing 1% NP40 instead of 1% Triton X-100. After centrifugation, the chromatin fraction was resuspended in 1 mL of the same buffer, and aliquots from the soluble and chromatin fractions were removed for the fractionation controls (H4 and Pgk1). The soluble and chromatin fractions were lysed with a Multi Beads Shocker at 4°C with 1x volume glass beads and the lysates were then processed as indicated for CoIP analyses.

Western blot

Protein samples were resolved by 8% (Mcm4-GFP, Mcm4-HA, Mcm7, Rad52-YFP, Rad51 and Rad52) or 15% (Pgk1 and H4) SDS-PAGE, and probed with antibodies against GFP (632381, Clontech), HA (Roche Refs: 11666606001 and 11867423001), Mcm4 (sc-166036, Santa Cruz), Mcm7 (sc-6688, Santa Cruz), Rad51 (sc-33626, Santa Cruz and ab63798, Abcam), Rad52 (Mortensen et al., 1996), Pgk1 (22C5D8, Invitrogen) or H4 (ab10158, Abcam). Yeast protein extracts to analyze total amount of Mcm4-GFP and Rad51 (Figure S4A) were prepared using the TCA protocol as described (Foiani et al., 1994). All western signals were acquired and quantified in a ChemiDoc MP image system and quantified with the Image Lab™ software (Biorad).

QUANTIFICATION AND STATISTICAL ANALYSIS

Image processing and analysis

The acquirement, processing and analysis of DNA repair foci, western blots, DNA fibers, and gels from 2D, ChEC and PFGE are specified in the corresponding Method details.

Statistical analyses

Statistical analyses were performed using the Prism software (GraphPad). Mean, SEM, sample size and statistical tests are indicated in the Figure legends. Sample size was not predetermined using statistical methods. Given the reduced sample size, the analyses were performed assuming that they follow normal distributions. Scatter SuperPlots were done as recently reported (Lord et al., 2020).